Contrib Mineral Petrol (1987) 95:420–436

Contributions to Mineralogy and Petrology


# The Brown Leucitic Tuff of Roccamonfina Volcano (Roman Region, Italy)

**James F. Luhr**[1] **and Bernardino Giannetti**[2]

[1] Department of Earth and Planetary Sciences, Washington University St. Louis, MO 63130, USA
[2] Centro di Studio per la Mineralogia e Petrologia delle Formazioni Ignee, C.N.R., c/o Dipartimento di Scienze della Terra Università "La Sapienza", I-Rome, Italy

**Abstract.** The Brown Leucitic Tuff (BLT) is a poorly to strongly lithified compositionally zoned pyroclastic-flow deposit with a minimum volume of 3 to 5 $km^3$. It erupted from Roccamonfina Volcano about 385000 years ago, after formation of the summit caldera. Individual flow units are grouped into three facies (white, brown, and orange) which primarily differ in pumice color, lithic content, and matrix cementation. Pumices from the BLT range from phonolitic leucite-tephrites to leucite-trachytes (7.0 to 2.2 wt% CaO), covering over half of the total spectrum of High-K Series magmas known from Roman Region volcanoes. White-facies units dominate in lower stratigraphic levels and their pumices have the lowest CaO contents, indicating a general trend toward more basic compositions as the eruption evolved. At higher stratigraphic levels, however, orange- and brown-facies units are interbedded with other white-facies units, indicating reversals in the dominant compositional progression.

BLT pumices have crystal contents of 9.9 to 0.6 vol%, with green salite > plagioclase > sanidine > biotite > titanomagnetite > analcime (after leucite) > apatite > pyrrhotite. In most samples, plagioclase ($An_{85-95}$) and sanidine ($Or_{75-90}$) have much lower $Na_2O$ contents than usually found in coexisting feldspars, yet these are interpreted as equilibrium pairs. Primary leucite has been almost completely replaced by analcime. All samples also contain xenocrysts of colorless diopside and forsteritic olivine ($Fo_{83-92}$). Recurrent alternations from colorless diopside to green salite are present in single clinopyroxene crystals and appear to reflect a complex history of magma mixing.

Whole-rock BLT pumice compositions conform closely to High-K Series lavas from Roccamonfina for all elements except $Na_2O$ and $K_2O$. The former is relatively enriched and the latter relatively depleted in mafic BLT pumices with > 5.6% CaO; these differences reflect strong analcimization of abundant groundmass leucite crystals in these pumices. Otherwise, major and trace element data support fractionation of observed minerals in generating the compositional diversity among BLT pumices. Mineral assemblages and compositions of cumulate monzonite and syenite nodules carried to the surface during the BLT eruption correspond closely to the fractionated phases predicted by least-squares modeling.

*Offprint requests to:* J.F. Luhr or B. Giannetti

## Introduction

The Roman Region of Italy is well known for the unusually potassic character of its Pliocene to Recent volcanism. Although numerous petrologic studies have been published regarding the lavas of the Roman Region, pyroclastic rocks, which often dominate volumetrically at the Italian volcanoes (Sparks 1975), have been essentially ignored in petrologic debates. The relative neglect of pyroclastic deposits in petrologic studies was also noted at a recent symposium on alkaline igneous rocks (Fitton and Upton 1985). We are currently involved in studies of the major pyroclastic deposits of Roccamonfina Volcano, which constitute some 70 to 80% of its erupted volume. In this paper we discuss the geology and petrology of an important pyroclastic-flow deposit, the Brown Leucitic Tuff (BLT), based on detailed mapping of the entire volcano and compositional data for pumices and constituent minerals from an extensive sample suite.

Roccamonfina lies 50 km NNW of Somma-Vesuvius along the western coast of Italy (Fig. 1). As is typical of Roman Region volcanoes, the growth of Roccamonfina was both long and petrologically complex. The history of the volcano is conveniently divided into two stages (Giannetti 1979a), which correspond in a general way to two distinct magma series: the leucite-rich High-K Series (HKS) of Stage I, and the leucite-poor to leucite-free K Series (KS) of Stage II. These two magma series were first identified by Appleton (1972) at Roccamonfina, and subsequently described from Vulsini (Varekamp 1980; Rogers et al. 1985) and Ernici (Civetta et al. 1981). Stage I activity constituted the major part of Roccamonfina's life; K-Ar ages for Stage-I products range from 1.54 to 0.34 million years (Giannetti et al. 1979). During this period, the main cone was constructed from repeated lava, pyroclastic-fall, and pyroclastic-flow eruptions accompanied by numerous mudflows. These materials span the HKS compositional spectrum from leucite tephrites (up to 13 wt% CaO) to phonolites (to 2% CaO), and are generally leucite bearing (Giannetti 1970, 1974). Pyroclastic activity, mainly involving phonolitic magmas, appears to have become dominant toward the close of Stage-I activity. A major pyroclastic-flow eruption near the end of Stage I, about 385000 years ago (Table 1), produced the compositionally zoned Brown Leucitic Tuff (BLT), which forms the subject of this paper. Rocca-

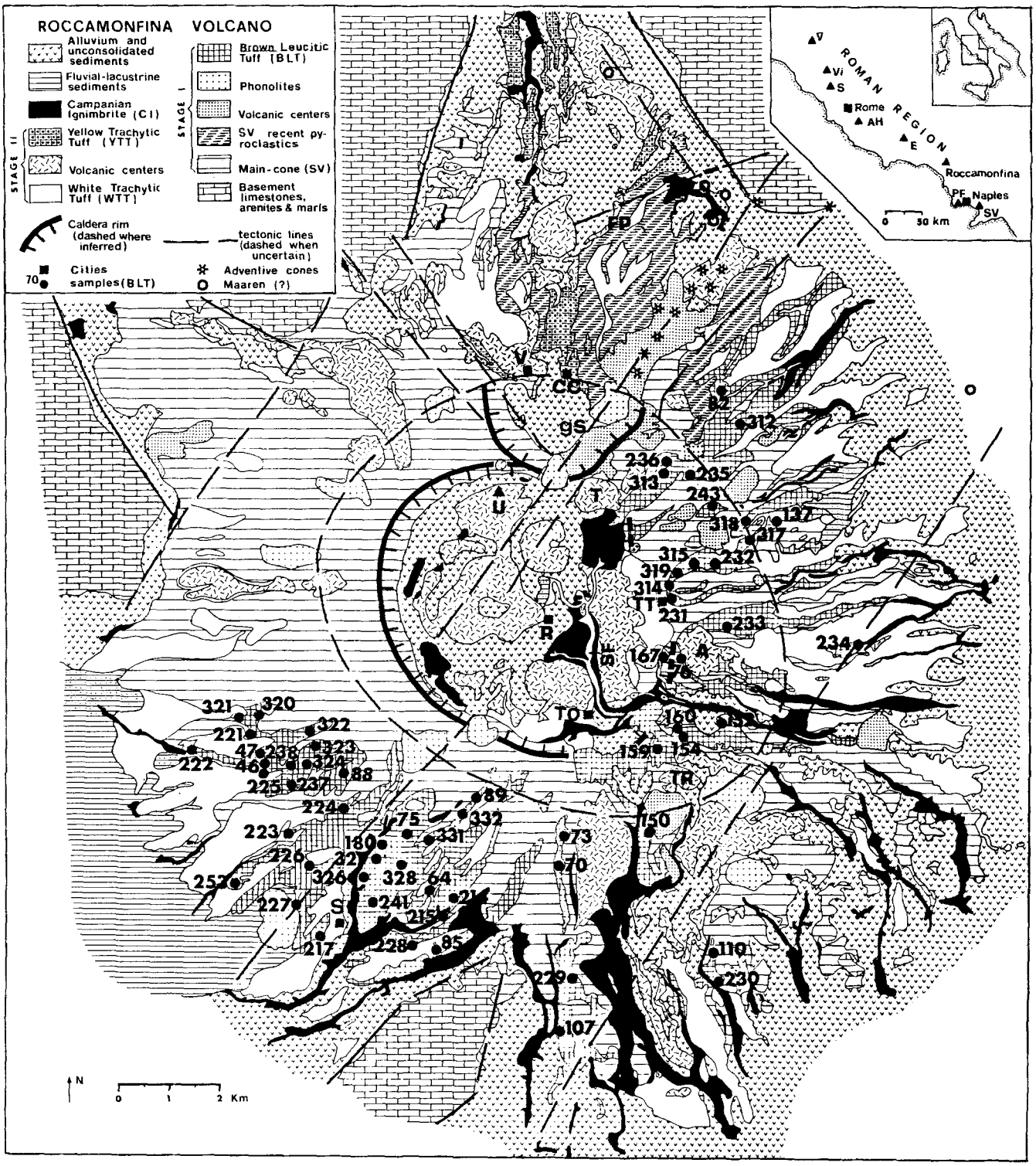


**Fig. 1.** Geologic map of Roccamonfina Volcano showing distribution of BLT. Key to geographic places: *TT* Tuoro di Tavola, *V* Vezzara, *CC* Conca Campania, *R* Roccamonfina, *TO* Torano, *S* Sessa Aurunca, *gS* 'gli Stagli' caldera, *TR* Mt. Triuci ejecta cone, *A* Mt. Atano ejecta cone, *T* Tuororame ejecta cone, *FP* Fosso Pubblico, *SF* Savone delle Ferriere ravine, *U* Unocal Geothermal Division drillhole Gallo 85-1

monfina presently has a well-developed summit caldera 5.5–6.5 km across and a smaller semicircular caldera (gli Stagli) which is tangent to the northern rim of the main one. As discussed below, the main caldera appears to have formed prior to the BLT activity, whereas 'gli Stagli' formed later. Although the BLT is often overlain by KS products, we have found up to 30 m of leucite-bearing HKS tephra above it as well. Thus the BLT did not signal the end of HKS activity.

We mark the beginning of Stage II activity at Roccamonfina with the eruption of the compositionally zoned White Trachytic Tuff (WTT) about 300000 years ago

**Table 1.** K-Ar age determinations for biotite and glass from BLT sample 47M

| Phase | UCB # | Sample wt (g) | $\%K^+$ | $\%^{40}Ar_{rad}$ | $^{40}Ar_{rad}$ (moles/g $\times 10^{-12}$) | Age (years) |
|---|---|---|---|---|---|---|
| Biotite | 4088R | 1.3447 | 7.414 | 5.5 | 4.956 | 385000+/−23000 |
| Glass | 4089 | 5.4637 | 2.69 | 21.5 | 1.314 | 282000+/− 7000 |

*UCB #* University of California Berkeley K-Ar Laboratory number

Decay constants: $\lambda_{40_{K_\beta}} = 4.962 \times 10^{-10}$/yr

$\lambda_{40_{K^e}} + \lambda'_{40_{K^e}} = 0.581 \times 10^{-10}$/yr

Isotopic abundance: $^{40}K = 0.01167\%\ K_{total}$

(Giannetti and Luhr 1983a). A complex sequence of pyroclastic eruptions then followed, mainly on the northern flank of the volcano, producing 'gli Stagli' caldera and a thick section of leucite-latite, leucite-basalt, and trachyte pyroclastic-fall and -flow deposits, culminating in the Yellow Trachytic Tuff (YTT: Fig. 1) and in the mudflow deposits of Conca Campania and Vezzara. Further leucite basalt, leucite latite, latite, trachybasalt, and basalt lava flows and domes erupted during this period on all parts of the volcano to bring the life of Roccamonfina to an apparent close. All of these Stage-II magmas belong to the K Series (KS) of the Roman Region, and with the exception of the leucite basalts and leucite latites they are leucite-free. Stage-II magmas are significantly depleted in K and related incompatible elements compared to Stage-I, HKS magmas (Appleton 1972) and have lower $^{87}Sr/^{86}Sr$ and higher $^{143}Nd/^{144}Nd$ and $^{206}Pb/^{204}Pb$ (Cox et al. 1976; Carter et al. 1978; Hawkesworth and Vollmer 1979; Vollmer and Hawkesworth 1980).

The most-recent volcanic event at Roccamonfina involved deposition of distal flow units from the Campanian Ignimbrite (CI: Giannetti 1964), a compositionally zoned pyroclastic-flow deposit which erupted about 30000 years ago in the Phlegraean Fields, some 50 km to the SSE (Di Girolamo 1970; Barberi et al. 1978, 1983; Cornell et al. 1979; Giannetti and Luhr 1983b).

## Field relations

### *Previous work*

Early contributions to the pyroclastic geology of Roccamonfina did not distinguish between the BLT and WTT, considering them as a single formation (Tedesco 1964; Bergomi et al. 1969). Di Girolamo (1968) was the first to recognize the BLT during his studies of the southwestern portion of Roccamonfina. Di Girolamo referred to the BLT as "Colate Piroclastiche Conglomeratiche di Sessa", correctly identifying it as a variably lithified pyroclastic-flow deposit containing pumices as well as abundant lithic fragments up to 1 m in diameter. Ghiara et al. (1973), however, later described the BLT (their Formation A) as a cold mudflow deposit, in conflict with the interpretations of Di Girolamo (1968) and of this study. As discussed below, this confusion is primarily a consequence of their misinterpretation of older Stage-I mudflow deposits on the western side of the volcano as belonging to the BLT. Giannetti (1979a and b) previously referred to the BLT as the "Yellow Leucitic Tuff", and this name is now superseded. In Fig. 1 of Giannetti and Luhr (1983a) we grouped the BLT with the YTT, which we now recognize as a younger pyroclastic-flow deposit (Fig. 1). More recently Chiesa et al. (1985) mistakenly took issue with our definition of the BLT, perhaps based on the absence of leucite in YTT pumices and in some crystal-poor BLT pumices. They also refer to the BLT event as a "Mount St. Helens type eruption" and correlate it with formation of the main caldera by eastward collapse of the main cone. No rockslide avalanche deposit exists on the eastern side of Roccamonfina, however, and as discussed below the main caldera appears to have formed prior to the BLT eruption. Thus, the hypothesis of Chiesa et al. (1985) appears to have little foundation.

**Fig. 2.** Brown-facies pyroclastic-flow unit of BLT near the town of Sessa Aurunca. Outcrop is very rich in lithic fragments and shows a fine-grained lens in the upper levels. Rock hammer for scale

### *BLT distribution and the calderas of Roccamonfina*

The BLT (Fig. 1) is found primarily on the southeastern half of the volcano where it forms tongues along radial ravines extending up to 7 km from the main caldera rim. In the east and south,

where the main caldera wall is low, the BLT extends up to the rim and into the caldera along the deep ravine of Savone delle Ferriere near Torano (Fig. 1). In the southwest, however, where the caldera wall rises progressively in a clockwise direction, the highest BLT outcrops are found at increasing distances from the rim, as also observed for the WTT (Giannetti and Luhr 1983a). Presumably this indicates erosion or non-deposition on the steep upper slopes of the main cone. Prior to BLT activity, Roccamonfina was dissected by numerous radial ravines cut up to 100 m deep into Stage-I lavas and pyroclastic deposits. These ravines were repeatedly filled and re-excavated with each of the subsequent major pyroclastic-flow eruptions. The well-lithified BLT and the variably lithified CI now crop out in the walls of ravines, whereas the poorly lithified WTT is usually restricted to radial ridges separating ravines. Sparks (1975) describes a similar process of drainage re-establishment following major pyroclastic-flow eruptions at Vulsini Volcano. BLT outcrops are scarce on the northern flank of Roccamonfina, but the WTT, the younger leucite latite tephra, and the overlying mudflow deposits of Conca-Vezzara contain abundant BLT xenoliths. Significantly, the BLT is absent in the west, behind the high wall of the main caldera. Fig. 2 of Ghiara et al. (1973) shows numerous outcrops of BLT on the western flank of the volcano which we interpret to be earlier Stage-I mudflow deposits.

The ages and origins of Roccamonfina's calderas are poorly known at present. The latite (KS) Tuororame ejecta cone lies along the northeast rim of the main caldera which it apparently postdates. This cone is overlain by BLT, demonstrating that: 1) KS and HKS magmas erupted alternately near the Stage I – Stage II transition, and 2) the main caldera formed prior to the BLT eruption, as previously concluded by Giannetti (1979b). Unocal Geothermal Division recently drilled a 900 m geothermal well (Gallo 85-1) in the northern part of the main caldera about 2.5 km NNW of Roccamonfina city (Fig. 1). It penetrated WTT (230 m), BLT (140 m), mudflow deposits, HKS lavas, and underlying bedded sediments containing limestone clasts, which mark the base of the volcano. The numerous pre-BLT mudflow deposits in this sequence also indicate caldera formation prior to the BLT eruption. The absence of BLT on the western flank of the volcano, behind the high wall of the main caldera, and the presence of BLT within the caldera near Torano, are also consistent with this interpretation. The smaller 'gli Stagli' caldera is interpreted to have formed later, following the WTT, during the complex sequence of pyroclastic eruptions which affected the northern flank of the volcano. These deposits and the caldera of 'gli Stagli' will be considered in detail elsewhere.

*Outcrop characteristics*

The BLT contains minor pyroclastic-fall and -surge units, but primarily consists of many interbedded pyroclastic-flow units (1 to 10 m in thickness) which can be roughly grouped into three major facies named for the outcrop color: white, brown, and orange (" ocra"). The facies differ principally in extent of alteration and lithification, pumice color, and lithic content. White units, which contain the most evolved (lowest-CaO) pumices, typically occupy the lowest stratigraphic positions and are followed upward by interbedded brown, orange, and minor white units.

White-facies units constitute about 20 vol% of the deposit and are best represented on the SW flank of Roccamonfina. The outcrop color results from an abundance of white pumices and ash and a relative scarcity of lithic fragments (<10 vol%). Great care must be exercised in order to avoid confusion between white-facies flow units of the BLT, other white HKS tephra units, and early flow units of the WTT. The latter can be positively distinguished only with close attention to stratigraphic position, recognition of its characteristic fine-grained basal surge layer, and by the absence of milk-white analcime which has replaced rare primary leucite in pumices of white-colored HKS tephra units. Low-angle cross-bedding of "surge" nature is present in the basal, white-facies flow units of the BLT, but these are generally not as abundant as those that characterize the basal WTT units (Giannetti and Luhr 1983a). The white-facies flow units of the BLT can be distinguished from other white-colored, analcime-bearing HKS units by the much greater thickness of the BLT units, and by the absence of pumice-fall layers which typify other HKS pyroclastics.

Brown-facies flow units constitute roughly 40% of the BLT and are also most abundant on the southwestern flank. These units are characterized by a brownish outcrop color, poor to moderate lithification, and an abundance of large lithic fragments which can exceed 1 m in diameter (Fig. 2). The brown units of the BLT, in fact, now appear to be the major source of the abundant cumulate nodules at Roccamonfina (Giannetti 1982). The percentage of lithics can vary widely, from 20 vol% to >80 vol% in lithic-rich lenses which are common at the base of flow units. Brown units also contain relatively basic (CaO-rich) pumices up to 40 cm in diameter that are grey to black when fresh, but typically show bleaching to a light-grey or beige color at the margins. In many outcrops, only the cores of the largest pumice clasts have escaped this alteration, smaller pumices being completely bleached. The abundance of pumices varies greatly in units of the brown facies, usually in inverse relation to the abundance of lithic fragments.

Flow units of the orange facies account for roughly 40% of the BLT and are most abundant on the northeastern flank of the volcano. They are characterized by their strongly lithified matrix, a relatively low content of lithic fragments (10 to 30 vol%), an essential absence of large lithic fragments, and the common alteration of pumices and matrix glass to an orange product which determines the outcrop color. Pumices are typically so rotten as to collapse when lightly squeezed between fingers, or else completely weathered out leaving holes in the outcrop. The marginal alteration of pumices in brown-facies units is apparently a precursor to the more-complete pumice alteration in orange units, and most orange-facies units are probably altered equivalents of brown units. The extensive alteration of pumices in the orange-facies flow units has essentially limited our petrologic studies to the white and brown facies, although a few relatively fresh pumices from orange units were also studied. The strong lithification of orange-facies flow units reflects cementation by chabazite which produces strong X-ray diffraction peaks only in orange facies matrix samples. Passaglia and Vezzalini (1985) document diagenetic chabazite and other zeolites from a variety of Italian pyroclastic deposits.

The BLT typically lies atop pyroclastic-fall and -flow deposits of earlier Stage-I activity. There are no obvious soils between these layers or between the various units of the BLT. Accordingly, the precise lower contact can be very difficult to discern. Up to 2 m of phonolitic pumice- and ash-fall layers underlie the lowest flow units of the BLT just W of Mt. Atano and at Tuoro di Tavola near the eastern rim of the main caldera (Fig. 1). These may represent an early Plinian phase of the BLT eruption as described for many other pyroclastic-flow-dominated events (Sparks et al. 1973). At other locations, however, the pyroclastic layers beneath the basal flow unit of the BLT appear typical of earlier Stage-I pyroclastic successions and these are interpreted to be unrelated to the BLT. We emphasize the relatively arbitrary nature of our lower BLT contact. The BLT appears to have been one of the closing acts of a long pyroclastic drama near the end of Stage-I activity. Other HKS tephra followed before Roccamonfina effectively completed its transition to KS magmas beginning with the WTT; HKS pyroclastics overlie the BLT along Fosso Pubblico in the north and on the path northwest of Triuci basaltic cinder cone (Fig. 1), and two published K-Ar dates for HKS lavas are younger than our age for the BLT (0.368 and 0.34 million years – Evernden and Curtis 1965; Cortini et al. 1975).

Where observable in the field, the BLT is either the surface formation or is overlain by the WTT or CI. Away from radial ravines the WTT either fills clean channels cut into the BLT, or is separated from the BLT by a paleo-soil up to 1 m thick. The presence of this paleo-soil is consistent with the 80000 year difference in their K-Ar ages (Table 1 and Giannetti and Luhr 1983a). From the absence of paleo-soils between flow units of the BLT, we infer that the entire eruption occurred within a relatively short time interval, probably less than several tens of years.

**Table 2.** Modal analyses determined by point counting (vol%)

| | 47M | 214 | 227 | 64 | 226 | 70.2G | 107B | 328-2 |
|---|---|---|---|---|---|---|---|---|
| San | 1.23 | 0.51 | 0.27 | 1.60 | 0.35 | 0.03 | 0.34 | 1.00 |
| Plag | 3.06 | 1.34 | 0.15 | 3.26 | 1.93 | 1.80 | 0.07 | 0.53 |
| Cpx | 4.25 | 2.90 | 0.10 | 3.71 | 2.76 | 2.33 | 0.16 | 0.33 |
| Biot | 0.91 | 1.28 | 0.15 | 1.52 | 1.19 | 0.79 | 0.02 | 0.14 |
| Tmt | 0.45 | 0.38 | 0.03 | 0.32 | 0.36 | 0.22 | 0.02 | 0.02 |
| Anal | n.d. | n.d. | n.d. | n.d. | n.d. | 0.10 | n.d. | n.d. |
| Crystals | 9.90 | 6.41 | 0.70 | 10.41 | 6.59 | 5.27 | 0.61 | 2.02 |
| Grndm | 90.10 | 93.59 | 99.30 | 89.59 | 93.41 | 94.73 | 99.39 | 97.98 |
| Vesicles | 27.17 | 31.71 | 16.25 | 23.92 | 22.38 | 14.03 | 15.85 | 27.73 |

Modes determined on epoxy-impregnated thin sections. Each analysis represents over 10000 points counted on three sections

Only crystals $>0.03$ mm are included. *n.d.* not detected but present as groundmass microlites

*Eruptive volume*

Given the valley-filling nature of the BLT and the lack of information concerning distal ashes, it is impossible to precisely reconstruct the eruptive volume. In ravines radiating from the main caldera, total thickness of the BLT can approach 80 m, but on radial ridges the original thickness may have been only 5 to 10 m. Present outcrops on the southeastern half of the volcano indicate a minimum depositional area of 160 $km^2$. Assuming an average thickness of 20 to 30 m, yields an estimated depositional volume of 3 to 5 $km^3$ for these proximal deposits. In converting to the erupted magma volume, these values will be reduced to account for the abundant lithic fragments in the BLT (30 to 40 vol%) and the reduced density of the deposit compared to the magma. These reductions are probably offset by the volume of distal ashes which have not been considered, however, and 3 to 5 $km^3$ is also our best estimate for the minimum BLT magma volume.

*K-Ar dating*

Phenocrystic biotite and matrix glass were separated from BLT pumice sample 47M and dated by the K-Ar method (Table 1). The biotite separate gives an age of $385000 \pm 23000$ years, which we believe represents the age of the BLT eruption. As discussed below, matrix glasses from BLT pumices contain abundant analcime crystals altered from primary leucite (Fig. 2). The significantly younger age determined on the groundmass glass of sample 47M ($282000 \pm 7000$ years) reflects this alteration history.

## Samples studied

Eighty four pumices were collected from the BLT for petrologic study. With the exception of the basal pumice-fall layers near Mt. Atano mentioned earlier, we have restricted our sampling to pyroclastic-flow units. Most pumices are from white- or brown-facies flow units; the majority of the highly altered orange-unit pumices were avoided. None of the pumices is pristine. In each, the groundmass glass has been hydrated and primary leucite has been mostly converted to analcime. It is precisely the ease of alteration of vesicular pumices that makes them less attractive than lavas for petrologic study. Yet when pyroclastic rocks constitute a large portion of the volcano, they can not be safely disregarded in petrologic models. Each of the pumices was analyzed by X-ray fluorescence techniques discussed in a following section. On the basis of these data we selected eight samples for further study including petrographic and electron microprobe analyses. Microprobe operating conditions are as discussed in Giannetti and Luhr (1983a). A sample current of 20 nA was used in analyzing glasses.

## Mineralogy

All BLT pumices contain a relatively simple assemblage of salite, plagioclase, sanidine, biotite, titanomagnetite (plus pyrrhotite inclusions), analcime (after leucite), and apatite, set in a colorless to brown vesicular glass. These minerals commonly form clusters which can be up to 3 mm across. Plagioclase and salite generally dominate in these clusters as they do among isolated phenocrysts.

Modes of crystal-poor pumices are inherently difficult to measure with accuracy. We determined modes for the selected BLT samples by conventional point counting of epoxy-impregnated pumices (Table 2). Total crystal contents range from $<1$ to 10 vol% and generally increase with whole-rock CaO content. Both mineral assemblages and mineral compositions are essentially constant within the sample suite; among the samples studied by microprobe, only 328-2, the least-calcic sample in the suite, shows slightly different mineral compositions. In all BLT pumices, relatively homogeneous salite crystals dominate the mafic assemblage. Some clinopyroxene crystals, however, have Mg-rich diopside cores or more complex compositional zoning patterns discussed below. All pumices also contain compositionally homogeneous xenocrysts of diopside and forsteritic olivine in small amounts.

*Plagioclase*

Euhedral plagioclase phenocrysts range up to 3 mm across in BLT pumices and typically have inclusions of brown glass and salite; other phenocrystic minerals are less common as inclusions. Individual crystals are essentially homogeneous in composition showing at most 2–3 mol% variation in An content. Rims are enriched in either Ca or Na. The great majority of crystals fall in the bytownite-anorthite compositional range ($An_{85-95}$), with a strong mode at $An_{87-89}$ (Fig. 3, Table 3). These calcic plagioclases also contain up to 1 wt% SrO. Sample 328-2, with only 316 ppm Sr in the whole rock, is dominated by Sr-poor andesine ($An_{45-50}$) with a few crystals of bytownite also present (Fig. 3, Table 3).

*Sanidine*

Phenocrysts of sanidine up to 2.5 mm long are mostly inclusion free, but rarely contain inclusions of any other phenocrystic mineral. Sanidine is usually subordinate to plagioclase, but dominates the felsic assemblage in crystal-poor pumices ($<2$ vol% crystals: samples 107B and 227 – Table 2). Individual sanidine crystals are generally homogeneous in composition with 75–90 mol% Or component (Table 3). The most-potassic sanidine crystals are associated with the most-calcic plagioclase in samples 214 and 227, and the most-sodic sanidine crystals coexist with the most-sodic plagioclases in sample 328-2. Tie lines between coexisting feldspars

**Table 3.** Representative microprobe analyses of feldspars

| Sample | 226 P | 226 S | 328-2 P | 328-2 S |
|---|---|---|---|---|
| Pts | 8 | 8 | 7 | 11 |
| Wt% | | | | |
| $SiO_2$ | 45.47 (0.55) | 63.61 (0.43) | 55.34 (0.87) | 63.98 (0.61) |
| $Al_2O_3$ | 34.39 (0.24) | 19.68 (0.23) | 28.30 (0.45) | 19.45 (0.22) |
| FeO | 0.69 (0.03) | 0.21 (0.03) | 0.34 (0.02) | 0.13 (0.02) |
| BaO | n.d. | 0.31 (0.26) | n.d. | n.d. |
| SrO | 0.76 (0.10) | 0.57 (0.10) | 0.08 (0.06) | 0.04 (0.03) |
| CaO | 17.41 (0.30) | 0.38 (0.05) | 9.80 (0.31) | 0.35 (0.06) |
| $Na_2O$ | 1.06 (0.17) | 1.27 (0.08) | 5.62 (0.17) | 2.26 (0.16) |
| $K_2O$ | 0.29 (0.09) | 14.26 (0.18) | 0.80 (0.05) | 13.41 (0.32) |
| Total | 100.07 | 100.29 | 100.28 | 99.62 |
| Mol fraction | | | | |
| An | 0.886 | 0.019 | 0.468 | 0.017 |
| Ab | 0.097 | 0.117 | 0.486 | 0.200 |
| Or | 0.017 | 0.864 | 0.046 | 0.783 |

*P* plagioclase, *S* sanidine. Analyses represent mean and one standard deviation (*parentheses*). *Pts* number of analyses included in mean; *n.d.* not detected

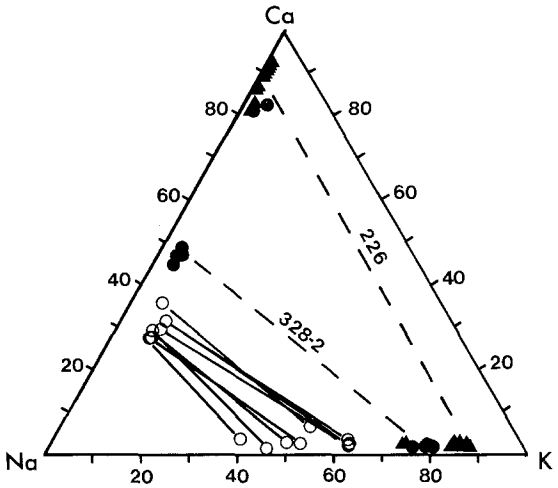


**Fig. 3.** Ternary feldspar plot (mol%) showing phenocryst analyses from sample 328-2 (*solid circles*) and all other BLT samples (*solid triangles*). *Dashed tie-lines* connect representative sanidine and plagioclase analyses from samples 328-2 and 226 (Table 3). *Open circles* with *solid tie-lines* are analyses of coexisting feldspars from Laacher See phonolites (Worner and Schmincke 1984a)

of the BLT pumices are shown on Fig. 3 along with the more-sodic coexisting feldspars of the Laacher See phonolites (Worner and Schmincke 1984a).

*Leucite-analcime*

All BLT pumices contain milk-white megascopic crystals of analcime which have replaced primary leucite phenocrysts. In addition, the more-basic BLT pumices (>5.6 wt% CaO) contain many small analcime crystals in the groundmass glass (Fig. 4). These are typically less than 0.02 mm across, but reach 0.25 mm in some pumices. Primary leucite is rarely preserved in the cores of larger crystals, but secondary analcime crystals can retain primary radial inclusion patterns of the leucite (Fig. 4). Analcimization of leucite, a common geologic phenomenon (Gupta and Fyfe 1975; Wilkinson 1977), caused significant increases in the Na/K ratios of basic BLT pumices as discussed in a later section. Because of the extreme Na-loss problems encountered in analyzing analcime, no analysis is reported for this phase.

**Table 4.** Representative microprobe analyses of biotite and apatite

| Sample | 47M Biot | 226 Biot | 328-2 Biot | 215 Ap |
|---|---|---|---|---|
| Pts | 8 | 7 | 6 | 4 |
| Wt% | | | | |
| $P_2O_5$ | n.a. | n.a. | n.a. | 40.37 (0.37) |
| $SiO_2$ | 35.27 (0.38) | 35.61 (0.42) | 35.27 (0.60) | 0.99 (0.07) |
| $TiO_2$ | 4.14 (0.10) | 3.97 (0.49) | 5.39 (0.15) | n.d. |
| $Al_2O_3$ | 15.07 (0.34) | 15.30 (0.37) | 14.87 (0.08) | 0.03 (0.02) |
| FeO | 15.24 (0.23) | 15.42 (0.35) | 16.58 (0.38) | 0.19 (0.03) |
| MnO | 0.17 (0.05) | 0.18 (0.03) | 0.25 (0.03) | 0.03 (0.01) |
| MgO | 14.60 (0.46) | 15.10 (0.49) | 13.96 (0.35) | 0.10 (0.02) |
| CaO | 0.03 (0.02) | 0.04 (0.02) | 0.03 (0.02) | 54.98 (0.23) |
| SrO | 0.15 (0.09) | n.d. | n.d. | 0.58 (0.05) |
| BaO | 0.49 (0.14) | 0.09 (0.11) | n.d. | n.d. |
| $Na_2O$ | 0.29 (0.03) | 0.33 (0.05) | 0.31 (0.04) | 0.23 (0.04) |
| $K_2O$ | 9.55 (0.11) | 9.68 (0.49) | 9.81 (0.18) | n.a. |
| F | 0.70 (0.05) | 0.50 (0.08) | 0.51 (0.06) | 2.41 (0.33) |
| Cl | n.d. | n.d. | n.d. | 0.16 (0.03) |
| $H_2O^a$ | 3.61 | 3.75 | 3.74 | 0.58 |
| $-O=F, Cl$ | 0.29 | 0.21 | 0.21 | 1.05 |
| Total | 99.02 | 99.76 | 100.51 | 99.60 |
| Mg # | 0.63 | 0.64 | 0.60 | – |

Analyses represent mean and standard deviation values (parentheses). *Pts* number of analyses included in mean; $H_2O^a$ calculated from stochiometry; *Mg #* Mg/(Mg+Fe); *n.d.* not detected; *n.a.* not analyzed

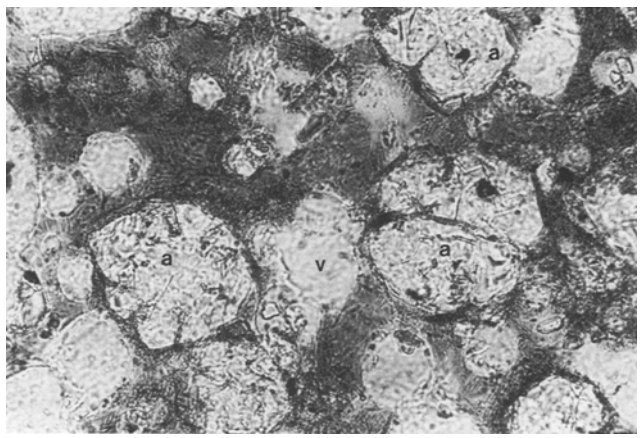


**Fig. 4.** Photomicrograph in plane light of inclusion-rich analcime crystals (*a*) and vesicles (*v*) in the groundmass glass of sample 47M. View is 0.25 mm across

*Biotite*

Biotite plates can reach 4 mm in length in BLT pumices. They typically contain apatite inclusions and are individually homogeneous in composition (Table 4) with Mg# (=Mg/(Mg+Fe))= 0.62 to 0.64. Biotites from CaO-poor sample 328-2 are slightly richer in Fe (Mg# =0.60).

*Apatite*

Prisms of apatite up to 0.5 mm long occur in the groundmass glass, and apatite needles are especially common as inclusions in biotite and salite phenocrysts. A representative microprobe analysis of Sr-F-rich apatite is given in Table 4.

**Table 5.** Representative microprobe analyses of titanomagnetite and pyrrhotite

| Sample | 47M | 226 | 328-2 | 328-2 |
|---|---|---|---|---|
| pts | 10 | 6 | 1 | 1 |
| Wt% | | | | |
| $SiO_2$ | 0.03 (0.02) | n.d. | n.d. | n.d. |
| $TiO_2$ | 5.22 (0.10) | 5.43 (0.04) | 6.55 | 4.28 |
| $Al_2O_3$ | 4.12 (0.23) | 4.25 (0.19) | 3.03 | 1.96 |
| $Cr_2O_3$ | 0.01 (0.02) | 0.02 (0.02) | 0.01 | n.d. |
| $V_2O_5$ | 0.45 (0.04) | 0.48 (0.04) | 0.51 | 0.44 |
| FeO | 81.15 (0.49) | 81.71 (0.56) | 82.30 | 86.39 |
| MnO | 0.65 (0.07) | 0.53 (0.04) | 0.77 | 0.60 |
| MgO | 2.07 (0.10) | 2.28 (0.08) | 1.85 | 0.41 |
| Total | 93.70 | 94.70 | 95.02 | 94.08 |
| $Fe_2O_3$ | 54.05 | 54.34 | 53.54 | 58.14 |
| FeO | 32.52 | 32.81 | 34.12 | 34.07 |
| Total | 99.12 | 100.14 | 100.38 | 99.90 |

Analyses for samples 47M and 226 represent mean and one standard deviation values (in parentheses). *Pts* number of analyses included in mean. Analyses for sample 328-2 are point analyses. $Fe_2O_3$ calculated after Carmichael (1967). *n.d.* not detected

| Sample | 160 |
|---|---|
| Wt% | |
| Fe | 60.70 |
| Cu | 0.19 |
| Mn | 0.03 |
| S | 38.74 |
| Total | 99.66 |
| Formula / 2 atoms | |
| Fe | 0.946 |
| Cu | 0.003 |
| Mn | 0.001 |
| S | 1.050 |

Pyrrhotite included in titanomagnetite

*Titanomagnetite*

Euhedral titanomagnetite phenocrysts up to 0.65 mm across occur in all BLT pumices and are common as inclusions in salite crystals. Most individual crystals are unzoned and show little compositional variation throughout the suite. Only sample 328-2 has titanomagnetites of varied composition (Table 5). Small pyrrhotite crystals are common in titanomagnetite crystals and are also homogeneous in composition throughout the suite (Table 5).

*Clinopyroxene (salite and diopside) and olivine*

The most abundant mafic mineral in BLT pumices is medium-dark green, pleochroic salite, forming stubby crystals up to 2 mm long and containing inclusions of brown glass, needle-like apatite, and titanomagnetite. Euhedral green salite crystals are usually homogeneous in composition, but complex zoning patterns occur rarely. In some crystals, light green to colorless diopside cores are abruptly surrounded by green salite mantles. A compositional profile across such a crystal is shown in Fig. 5. In a few such crystals, up to three repeated, abrupt alternations from colorless diopside to green salite were observed.

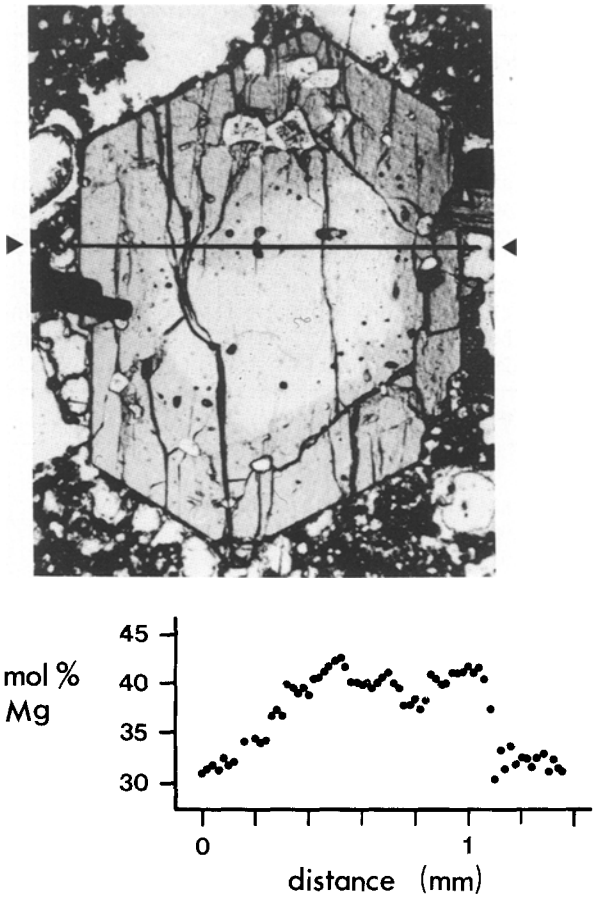


**Fig. 5.** Electron microprobe compositional zoning profile through a salite phenocryst with large diopside core in sample 64. Right side of profile shows an abrupt increase in Mg. The gradual increase on the left side probably indicates that the compositional interface is at a high angle to the beam path

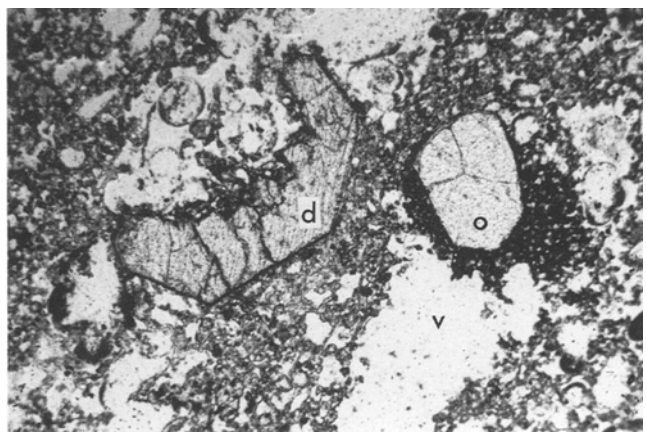


**Fig. 6.** Photomicrograph in plane light of partially resorbed diopside (*d*) and subhedral olivine (*o*) xenocrysts in sample 227. Both xenocrysts are partially surrounded by dark, microcrystalline groundmass material that is texturally distinct from the normal groundmass. View is 2.6 mm across

In addition to the salite phenocrysts, rare homogeneous light-green to colorless diopside crystals are present in all BLT pumices. These diopside crystals can reach very large sizes (→ 2 cm) and

**Table 6.** Representative microprobe analyses of clinopyroxene and olivine

| Sample | 47M | 328-2 | 328-2 | 226 | 64 | 328-2 | 328-2 | 64 | 47M | 214 | 328-2 |
|---|---|---|---|---|---|---|---|---|---|---|---|
| | a | b | c | d | e | f | g | h | i | j | k |
| Wt% | | | | | | | | | | | |
| $SiO_2$ | 52.51 | 48.43 | 46.75 | 47.83 | 46.73 | 44.63 | 43.51 | 40.17 | 40.47 | 40.53 | 39.46 |
| $TiO_2$ | 0.33 | 0.84 | 1.05 | 1.02 | 1.04 | 1.60 | 1.39 | n.a. | n.a. | n.a. | n.a. |
| $Al_2O_3$ | 1.57 | 5.82 | 6.04 | 5.67 | 6.33 | 6.94 | 7.79 | n.a. | n.a. | n.a. | n.a. |
| FeO | 3.04 | 6.04 | 9.64 | 10.49 | 10.87 | 13.09 | 16.83 | 9.35 | 10.00 | 10.93 | 16.17 |
| MnO | 0.06 | 0.13 | 0.26 | 0.33 | 0.28 | 0.57 | 1.06 | 0.18 | 0.15 | 0.21 | 0.27 |
| MgO | 17.45 | 14.28 | 11.85 | 11.26 | 11.15 | 9.12 | 6.42 | 49.30 | 48.76 | 47.75 | 43.55 |
| CaO | 24.15 | 23.72 | 23.46 | 23.70 | 23.82 | 22.90 | 22.22 | 0.42 | 0.39 | 0.43 | 0.23 |
| $Na_2O$ | 0.13 | 0.19 | 0.40 | 0.47 | 0.44 | 0.57 | 0.88 | n.a. | n.a. | n.a. | n.a. |
| Total | 99.24 | 99.45 | 99.45 | 100.77 | 100.66 | 99.42 | 100.10 | 99.42 | 99.77 | 99.85 | 99.68 |
| Mol fraction | | | | | | | | | | | |
| Fe | 0.047 | 0.098 | 0.159 | 0.172 | 0.177 | 0.223 | 0.296 | 0.096 | 0.103 | 0.114 | 0.172 |
| Mg | 0.478 | 0.411 | 0.347 | 0.330 | 0.324 | 0.277 | 0.202 | 0.904 | 0.897 | 0.886 | 0.828 |
| Ca | 0.475 | 0.491 | 0.494 | 0.498 | 0.499 | 0.500 | 0.502 | – | – | – | – |

Letters *a–k* indicate analyses on Fig. 7. *n.a.* not analyzed

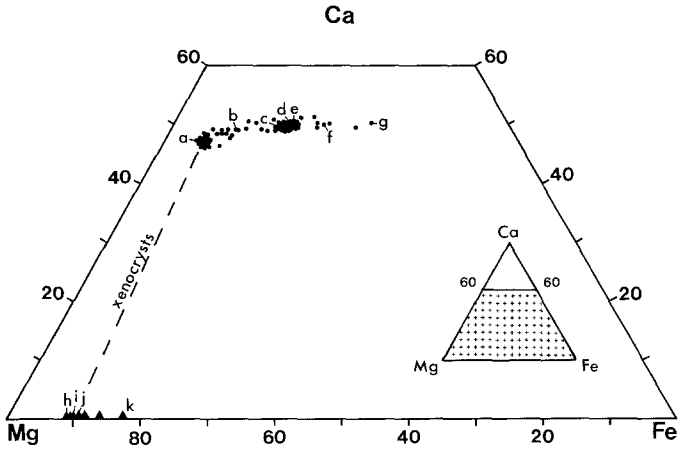


**Fig. 7.** Clinopyroxene and olivine compositions from BLT samples plotted on the lower portion of the pyroxene quadrilateral (mol%). Letters *a–g* and *h–k* indicate analyses of clinopyroxenes and olivine respectively from Table 6

**Table 7.** Representative microprobe analyses of glass

| Sample | 64 | 226 | 226 | 328-2 |
|---|---|---|---|---|
| type | Matrix | Matrix | Glass inclusion | Matrix |
| Pts | 6 | 8 | 4 | 5 |
| Wt% | | | | |
| $SiO_2$ | 55.96 (0.79) | 57.02 (0.53) | 56.00 (0.49) | 55.66 (0.32) |
| $TiO_2$ | 0.52 (0.03) | 0.45 (0.03) | 0.42 (0.03) | 0.35 (0.04) |
| $Al_2O_3$ | 19.85 (0.35) | 20.04 (0.29) | 19.48 (0.60) | 22.33 (0.14) |
| FeO | 4.17 (0.27) | 3.22 (0.14) | 3.57 (0.63) | 1.88 (0.07) |
| MnO | 0.15 (0.03) | 0.15 (0.01) | 0.13 (0.02) | 0.07 (0.02) |
| MgO | 0.80 (0.09) | 0.53 (0.05) | 0.53 (0.09) | 0.45 (0.05) |
| CaO | 4.36 (0.61) | 3.41 (0.22) | 3.09 (0.46) | 1.89 (0.13) |
| SrO | 0.22 (0.09) | 0.13 (0.05) | 0.10 (0.02) | 0.05 (0.06) |
| $Na_2O$ | 3.16 (0.60) | 2.91 (0.19) | 2.84 (0.38) | 3.96 (0.29) |
| $K_2O$ | 7.04 (0.28) | 8.85 (0.43) | 9.21 (0.15) | 7.51 (0.09) |
| Total | 96.23 | 96.71 | 95.37 | 94.15 |
| CIPW norm (Wt%) | | | | |
| Or | 43.33 | 54.15 | 57.13 | 47.16 |
| Ab | 26.36 | 19.69 | 16.18 | 32.85 |
| An | 19.99 | 16.03 | 13.86 | 9.96 |
| Ne | 0.80 | 3.14 | 4.90 | 1.49 |
| C | – | – | – | 4.52 |
| Di | 2.19 | 1.28 | 1.93 | – |
| Ol | 6.29 | 4.81 | 5.16 | 3.30 |
| Ilm | 1.03 | 0.88 | 0.84 | 0.71 |

Analyses represent mean and one standard deviation (*parentheses*). *Pts* number of analyses included in mean

are typically euhedral to subhedral, but some show cusp-shaped dissolution features (Fig. 6). In rare instances, diopside forms clusters which forsteritic olivine ($Fo_{82-91}$), which is euhedral to anhedral and can show iddingsite fracture fillings and rims. These diopside and olivine crystals are viewed as xenocrysts in BLT pumices. They are characteristically free of inclusions and sometimes are rimmed by dark-brown, microcrystalline groundmass material which is easily distinguished from the light-brown groundmass glass of BLT pumices (Fig. 6). Similar diopside and Mg-olivine xenocrysts are also present in most WTT pumices (Giannetti and Luhr 1983a).

Representative analyses of clinopyroxene and olivine are listed in Table 6 and plotted on Fig. 7. Salites cluster strongly in the range $Ca_{49-51}Mg_{31-34}Fe_{16-19}$, with some more iron-rich crystals present. Diopsides cluster near $Ca_{47}Mg_{47}Fe_6$, although all intermediate compositions between the dominant diopside and salite are represented.

*Glass*

Groundmasses of BLT pumices consist of vesicular colorless to brown glass, which in the more-basic samples (>5.6% CaO) contains abundant small analcime crystals. Many samples show fine-scale blending of the colorless and brown glasses. In such pumices, no compositional differences could be detected between them; the color of brown glasses may be due to cryptocrystalline titanomagnetite. Many groundmass glasses gave Q- or C-normative analyses, probably due to post-eruptive alteration and to volatization of alkalies during electron bombardment (Nielsen and Sigurdsson 1981). No attempt was made to correct for this problem. In addi-

**Table 8.** Representative whole-rock pumice compositions by X-ray fluorescence

| Sample | 47M | 214 | 227 | 64 | 226 | 70.2G | 107B | 328-2 |
|---|---|---|---|---|---|---|---|---|
| facies | B | B | B | B | B | B | W | W |
| (Wt%) | | | | | | | | |
| $SiO_2$ | 52.72 | 53.27 | 52.90 | 52.93 | 53.85 | 54.50 | 55.24 | 54.87 |
| $TiO_2$ | 0.62 | 0.61 | 0.60 | 0.57 | 0.52 | 0.49 | 0.39 | 0.26 |
| $Al_2O_3$ | 18.09 | 18.89 | 18.65 | 18.79 | 19.22 | 19.15 | 19.92 | 20.87 |
| $Fe_2O_3$ | 3.60 | 3.73 | 3.66 | 3.30 | 2.30 | 2.47 | 1.73 | 1.40 |
| FeO | 2.56 | 1.94 | 1.98 | 1.81 | 2.16 | 1.77 | 1.27 | 1.08 |
| ($FeO^T$) | (5.80) | (5.30) | (5.27) | (4.78) | (4.23) | (3.99) | (2.83) | (2.34) |
| MnO | 0.12 | 0.13 | 0.12 | 0.12 | 0.11 | 0.11 | 0.13 | 0.13 |
| MgO | 2.62 | 2.15 | 2.25 | 1.85 | 1.78 | 1.42 | 0.57 | 0.53 |
| CaO | 6.74 | 6.09 | 5.99 | 5.44 | 4.77 | 4.19 | 2.72 | 2.29 |
| $Na_2O$ | 5.14 | 6.34 | 5.57 | 4.47 | 3.81 | 4.40 | 3.99 | 4.74 |
| $K_2O$ | 3.63 | 2.25 | 3.56 | 5.26 | 8.07 | 6.97 | 8.74 | 8.51 |
| $P_2O_5$ | 0.28 | 0.23 | 0.25 | 0.21 | 0.20 | 0.15 | 0.09 | 0.05 |
| LOI | 3.77 | 4.31 | 4.81 | 4.48 | 3.62 | 4.50 | 4.81 | 5.29 |
| Total | 99.89 | 99.94 | 100.34 | 99.23 | 100.41 | 100.12 | 99.60 | 100.02 |
| CIPW norm (Wt%) | | | | | | | | |
| Or | 22.32 | 13.90 | 22.02 | 32.81 | 49.27 | 43.08 | 54.49 | 53.09 |
| Ab | 33.53 | 44.91 | 36.62 | 29.38 | 12.26 | 23.71 | 18.83 | 18.09 |
| An | 16.20 | 17.19 | 16.09 | 16.54 | 11.89 | 12.46 | 11.22 | 11.12 |
| Ne | 6.35 | 6.06 | 6.89 | 5.71 | 11.40 | 8.25 | 9.09 | 13.14 |
| Di | 13.19 | 10.00 | 10.37 | 8.18 | 8.98 | 6.54 | 1.93 | 0.43 |
| Ol | 1.09 | 0.67 | 0.74 | 0.75 | 1.25 | 0.88 | 0.79 | 1.35 |
| Mt | 5.43 | 5.13 | 5.27 | 4.83 | 3.45 | 3.75 | 2.65 | 2.14 |
| Ilm | 1.22 | 1.21 | 1.19 | 1.14 | 1.02 | 0.97 | 0.78 | 0.52 |
| Hm | 0.00 | 0.36 | 0.20 | 0.15 | 0.00 | 0.00 | 0.00 | 0.00 |
| Ap | 0.68 | 0.56 | 0.61 | 0.52 | 0.48 | 0.36 | 0.22 | 0.12 |
| (ppm) | | | | | | | | |
| V | 127 | 123 | 146 | 117 | 100 | 100 | 67 | 29 |
| Cu | 20 | 8 | 17 | 9 | 8 | 5 | 3 | 6 |
| Zn | 75 | 68 | 72 | 80 | 70 | 73 | 80 | 89 |
| Ga | 17 | 22 | 22 | 19 | 21 | 22 | 19 | 23 |
| Rb | 602 | 597 | 801 | 477 | 457 | 533 | 500 | 405 |
| Sr | 1706 | 1601 | 1538 | 1441 | 1344 | 1172 | 515 | 316 |
| Y | 42 | 43 | 47 | 39 | 38 | 46 | 47 | 40 |
| Zr | 254 | 312 | 307 | 320 | 317 | 341 | 416 | 491 |
| Nb | 23 | 23 | 22 | 25 | 24 | 26 | 27 | 34 |
| Cs | 31 | 45 | 35 | 51 | 35 | 55 | 45 | 41 |
| Ba | 793 | 827 | 790 | 695 | 690 | 548 | 235 | 179 |
| La | 77 | 101 | 92 | 93 | 104 | 100 | 144 | 162 |
| Ce | 197 | 204 | 191 | 201 | 211 | 209 | 233 | 264 |
| Pb | 54 | 48 | 45 | 53 | 46 | 57 | 65 | 140 |
| Th | 38 | 45 | 42 | 51 | 39 | 47 | 64 | 105 |

Facies: *B* brown, *W* white.

Major elements determined on fused glass disks following a modification of the technique of Rose et al. (1963). Trace elements determined on pressed powder disks. Trace element uncertainties in Giannetti and Luhr (1983a)

tion to groundmass glasses, glass inclusions in phenocrysts were also analyzed. These have compositions that are indistinguishable from the groundmass glasses. Representative glass analyses and CIPW norms are given in Table 7. Unfortunately, no analysis could be obtained for the vesicular dark brown groundmass material adhering to diopside and olivine xenocrysts (Fig. 6).

## Whole-rock compositions

Locations for the eighty four collected pumices are indicated on Fig. 1. Each sample is a single pumice lump. These were cleaned and crushed in a SPEX shatterbox container of tungsten carbide and analyzed for major and trace elements by X-ray fluorescence (XRF). Twenty seven samples were disregarded because of excessive alteration reflected in high values of LOI (>6.5 wt%), $SiO_2$, $Al_2O_3$, and normative Q, Hy, and C. The remaining fifty seven pumices have LOI from 3.3 to 6.5 wt% and normative Ne, Ol, and Di. We believe that these normative characteristics applied to all BLT pumices upon eruption. XRF analyses and CIPW norms are given in Table 8 for eight representative BLT pumices. Additional trace element data determined

**Table 9.** Instrumental neutron activation analyses of BLT pumices

| Sample | 47M | | 214 | | 227 | | 227 | | 64 | | 226 | | 70.2G | | 107B | | 328-2 | |
|---|---|---|---|---|---|---|---|---|---|---|---|---|---|---|---|---|---|---|
| facility | LBL | | WU | | WU | | LBL | | WU | | WU | | WU | | WU | | LBL | |
| (ppm) | | | | | | | | | | | | | | | | | | |
| Sc | 9.48 | (0.09) | 6.39 | (0.06) | 8.09 | (0.08) | 9.01 | (0.09) | 6.90 | (0.07) | 5.53 | (0.06) | 4.03 | (0.04) | 1.01 | (0.01) | 1.70 | (0.02) |
| Cr | 27.7 | (0.6) | 37.8 | (0.6) | 24.5 | (0.6) | 28.2 | (0.9) | 15.6 | (0.9) | 22.9 | (0.5) | 12.1 | (0.4) | 1.7 | (0.3) | 5.9 | (0.7) |
| Co | 12.0 | (0.2) | 11.0 | (0.1) | 11.0 | (0.1) | 12.1 | (0.2) | 9.1 | (0.2) | 8.0 | (0.1) | 6.66 | (0.09) | 2.52 | (0.06) | 2.2 | (0.1) |
| Sb | 0.94 | (0.09) | 0.56 | (0.03) | 0.77 | (0.05) | 0.79 | (0.09) | 0.77 | (0.05) | 0.83 | (0.03) | 1.00 | (0.05) | 1.75 | (0.07) | 2.8 | (0.2) |
| Cs | 32.9 | (0.6) | 39.9 | (0.4) | 37.0 | (0.4) | 38.3 | (0.6) | 39.7 | (0.4) | 33.7 | (0.4) | 66.0 | (0.7) | 47.7 | (0.5) | 40.8 | (0.7) |
| Ba | 852 | (14) | 781 | (25) | 760 | (25) | 727 | (22) | 723 | (26) | 633 | (22) | 521 | (18) | 192 | (11) | 177 | (18) |
| La | 101.6 | (0.8) | 94.0 | (0.9) | 93.3 | (0.9) | 103 | (1) | 94.4 | (1.0) | 99 | (1) | 97.9 | (1.0) | 124.3 | (1.3) | 164 | (2) |
| Ce | 212 | (2) | 193 | (2) | 195 | (2) | 208 | (1) | 194 | (2) | 198 | (2) | 202 | (2) | 240 | (3) | 275 | (2) |
| Nd | 93 | (2) | 84 | (2) | 85 | (3) | 80 | (2) | 82 | (3) | 82 | (3) | 86 | (2) | 86 | (4) | 66 | (2) |
| Sm | 14.0 | (0.1) | 13.7 | (0.2) | 13.4 | (0.3) | 13.2 | (0.1) | 12.9 | (0.3) | 13.2 | (0.3) | 12.4 | (0.2) | 12.5 | (0.2) | 8.16 | (0.08) |
| Eu | 3.34 | (0.03) | 2.61 | (0.04) | 2.70 | (0.04) | 2.79 | (0.02) | 2.47 | (0.03) | 2.45 | (0.03) | 2.32 | (0.03) | 1.84 | (0.02) | 1.25 | (0.01) |
| Tb | 1.28 | (0.04) | 1.31 | (0.04) | 1.34 | (0.04) | 1.17 | (0.02) | 1.29 | (0.04) | 1.31 | (0.04) | 1.24 | (0.03) | 1.19 | (0.03) | 0.59 | (0.02) |
| Dy | – | – | – | – | – | – | 6.7 | (0.2) | – | – | – | – | – | – | – | – | 4.7 | (0.2) |
| Yb | 3.13 | (0.05) | 2.80 | (0.06) | 2.89 | (0.05) | 3.07 | (0.04) | 2.71 | (0.06) | 2.93 | (0.06) | 3.03 | (0.06) | 3.39 | (0.06) | 3.93 | (0.04) |
| Lu | 0.43 | (0.01) | 0.41 | (0.01) | 0.44 | (0.01) | 0.42 | (0.02) | 0.44 | (0.01) | 0.45 | (0.01) | 0.45 | (0.01) | 0.53 | (0.01) | 0.55 | (0.03) |
| Hf | 6.8 | (0.1) | 6.6 | (0.1) | 6.8 | (0.1) | 6.79 | (0.08) | 6.8 | (0.1) | 6.7 | (0.1) | 7.4 | (0.1) | 8.9 | (0.1) | 10.17 | (0.09) |
| Ta | 1.31 | (0.01) | 1.32 | (0.03) | 1.29 | (0.03) | 1.21 | (0.01) | 1.40 | (0.03) | 1.41 | (0.03) | 1.58 | (0.03) | 1.27 | (0.03) | 1.41 | (0.01) |
| W | 5.5 | (0.5) | – | – | 10.9 | (1.3) | 6.4 | (1.1) | 9.5 | (1.2) | – | – | – | – | 9.4 | (1.0) | 6.3 | (1.2) |
| Th | 38.2 | (0.2) | 37.6 | (0.4) | 37.2 | (0.4) | 40.1 | (0.4) | 38.7 | (0.4) | 39.3 | (0.4) | 44.9 | (0.5) | 57.2 | (0.6) | 104 | (1) |
| U | 7.72 | (0.04) | 7.3 | (0.3) | 8.5 | (0.2) | 8.21 | (0.08) | 9.0 | (0.3) | 9.6 | (0.3) | 10.2 | (0.3) | 15.5 | (0.4) | 24.3 | (0.2) |
| Eu/Eu* | 0.82 | | 0.65 | | 0.68 | | 0.73 | | 0.64 | | 0.63 | | 0.63 | | 0.50 | | 0.56 | |

Facility: *LBL* Lawrence Berkeley Laboratory (Perlman and Asaro 1969); *WU* Washington University (Jacobs et al. 1977; Lindstrom and Korotev 1982). *Numbers in parentheses* represent counting uncertainties of one standard deviation. *Eu** interpolated between chondrite-normalized values for Sm and Tb

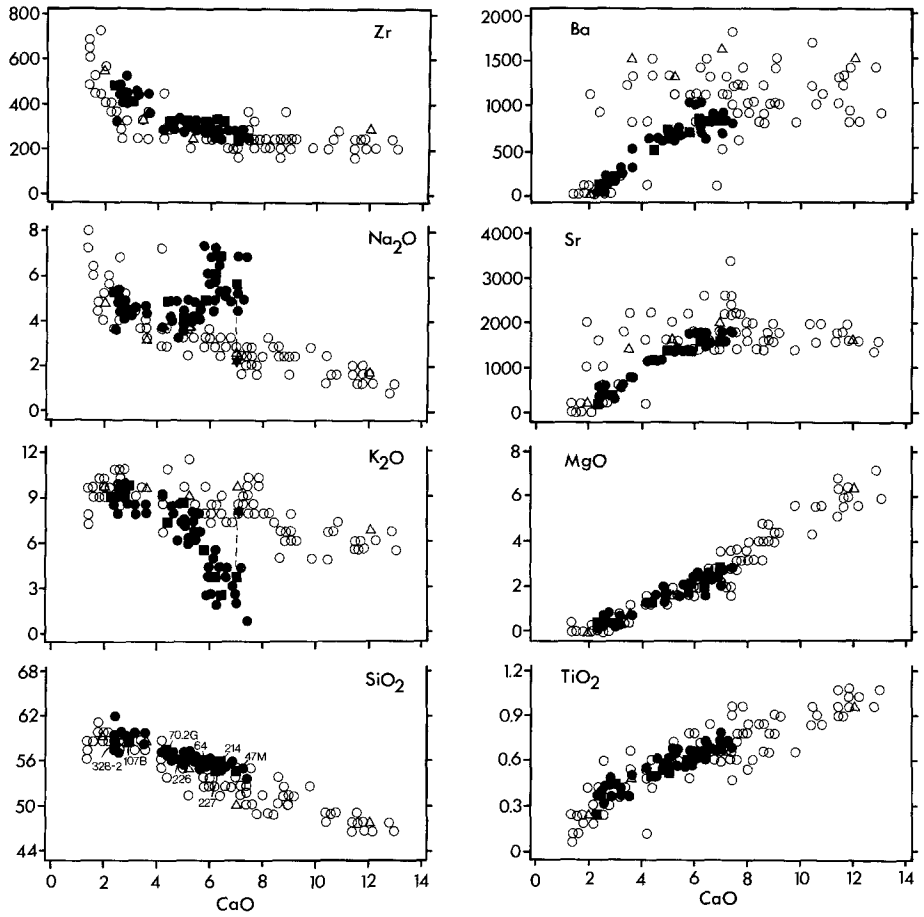


**Fig. 8.** CaO-variation diagrams for fifty-seven BLT pumices in *solid symbols*. *Squares* indicate samples from Table 8 which are labeled on the $CaO$-$SiO_2$ plot. On $Na_2O$ and $K_2O$ plots, *stars* indicate presumed primary composition of sample 47M. *Open circles* represent 80 unpublished wet-chemical analyses of HKS lavas. Trends of the latter are very similar to those of Appleton (1972). The chemical variations of BLT pumices closely match those for lavas, except for the alkalies, whose symmetrically deviant behavior is related to analcimization of leucite. For clarity, data symbols are larger than most analytical errors

by instrumental neutron activation (INA) for agate-ground splits from these samples are listed in Table 9. In the following discussion, all major element data are normalized to 100 wt% volatile free to avoid problems related to variable hydration. We use CaO as a petrologic index variable for reasons discussed in Giannetti and Luhr (1983a).

Current nomenclature for potassic volcanic rocks generally applies modes or Rittmann norms (Rittmann 1973) to the QAPF classification system of Streckeisen (1967). On the basis of Rittmann norms, analcime-poor BLT pumices range from *phonolitic leucite-tephrite* to *tephritic leucite-phonolite* to *leucite-trachyte*. As a consequence of the alteration of primary leucite, analcime-rich BLT pumices are displaced from the primary trend to the fields for basalt to latite. Progressing from the most-basic (47M) to the most-evolved (328-2) pumice, CaO decreases smoothly from 7.4 to 2.4 wt%. The other elements can be divided into three groups on the basis of their behavior in this progression:

Group I – Positively correlated with CaO: $TiO_2$, $FeO^T$, MgO, $P_2O_5$, V, Cu, Sr, Ba, Sc, Cr, Co, Nd, Sm, Eu, and Tb

Group II – Negatively correlated with CaO: $SiO_2$, $Al_2O_3$, $K_2O$, Zr, Nb, La, Ce, Yb, Lu, Pb, Th, Sb, Hf, and U

Group III – Constant or irregular behavior with CaO: $Na_2O$, Mn, Zn, Ga, Y, Cs, Ta, and Rb

Representative elements from Groups I and II are plotted on CaO variation diagrams in Fig. 8, along with data for eighty HKS lavas and scoriae from Roccamonfina (unpublished data). Pumices from this single eruption span approximately half of the entire HKS magma spectrum. For many elements (e.g., Mg and Ti), BLT trends conform closely to those of HKS lavas. Important deviations are shown by the alkalies, however, with $Na_2O$ relatively enriched and $K_2O$ relatively depleted in basic (>5.6% CaO) BLT pumices. These deviations are clearly related to widespread analcimization of abundant small leucite in these basic pumices. Analcimization of leucite probably also modified concentrations of Rb and Cs, two elements that are concentrated in leucite (Peccerillo et al. 1984) and that increase strongly during analcimization of leucite (Fornaseri and Penta 1960). These elements show wide scatter on CaO-variation diagrams for BLT samples.

There is a relative scarcity of both BLT pumices and HKS lavas at 3.8% CaO (Fig. 8). Interestingly, many elements including Zr, Ba, and Sr show slight deflections in trend at this point when plotted against CaO. These features are discussed in the next section.

A chondrite-normalized rare earth element (REE) plot for BLT pumices is shown in Fig. 9. In general, the light (La, Ce) and heavy (Yb, Lu) REEs increase and the middle REEs (Sm, Eu, Tb) decrease as CaO decreases through the suite from sample 47M to sample 328-2. As discussed in the next section, these trends are consistent with fractionation of an assemblage with middle-REE-enriched salite and apatite controlling REE concentrations. The patterned field represents leucite-tephrite lavas, the most primitive

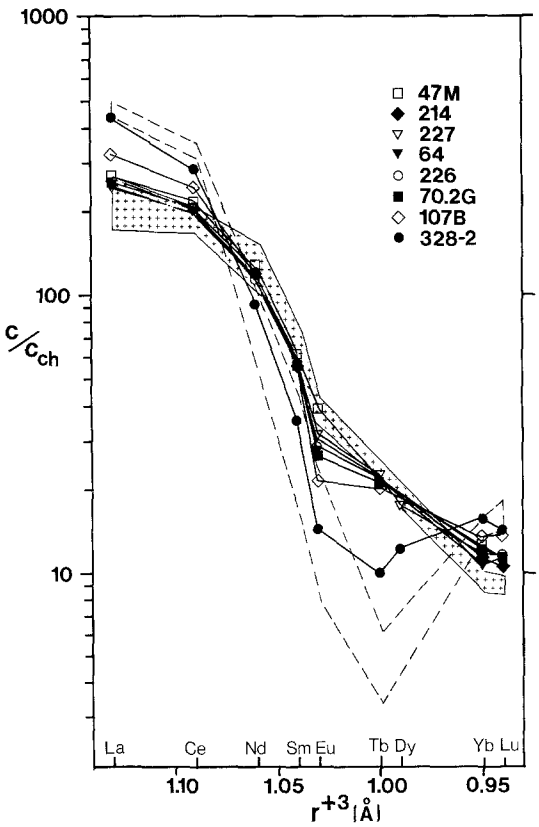


**Fig. 9.** Chondrite-normalized rare earth element plot for eight BLT pumices (Table 9) referenced to the Leedy Chondrite (Masuda et al. 1973). Ionic radii taken from Whittaker and Muntus (1970). *Patterned field* represents leucite tephrites from Roccamonfina (unpublished data), presumably parental to the BLT pumices. *Dashed lines* indicate the predicted pattern for sample 328-2 according to the crystal fractionation model of Table 10

members of the HKS (unpublished data), which are smoothly continuous with basic BLT pumices, supporting a parental relationship to the latter.

Wherever possible, pumices from stratigraphically related pyroclastic-flow units were collected to test for changes in magma composition with time through the eruption. White-facies flow units which are most abundant at the lowest stratigraphic levels, contain relatively evolved pumices (<4 wt% CaO), whereas overlying brown units typically contain more basic pumices with >4 wt% CaO. Thus, in a general way the BLT can be modeled as an inverted compositionally zoned magma chamber with magma compositions becoming progressively more basic as the eruption evolved (Hildreth 1981; Giannetti and Luhr 1983a, b). In detail, however, the pattern is more complex, as evidenced by interbedded brown, orange, and white units in some upper sections. Nine pairs of pumices from stratigraphically successive pyroclastic-flow units were studied in order to deduce compositional trends with time. Six of these show normal zoning, with the upper pumice more calcic. Two pairs show reverse zoning, and one shows no significant change in pumice composition. Although individual BLT outcrops are dominated by a single variety of pumice, through careful searching it is usually possible to find several different pumice types and compositions represented. Thus magmas from different portions of the compositionally zoned magma chamber were apparently erupted synchronously as modeled by Blake (1981) and Spera et al. (1986).

## Discussion

### *Two-feldspar equilibrium*

BLT pumices contain isolated euhedral plagioclase and sanidine phenocrysts which typically show little compositional variation. These two minerals are also present in crystal clusters with salite, titanomagnetite, and biotite, and have the same minerals as inclusions. There can be no doubt that plagioclase and sanidine were crystallizing in equilibrium in BLT magmas prior to eruption, and in principal, equilibration temperatures can be calculated from two-feldspar geothermometry.

Numerous formulations of the two-feldspar geothermometer have been proposed in recent years (Stormer 1975; Brown and Parsons 1981; Haselton et al. 1983; Ghiorso 1984), based primarily on the experimental data of Seck (1971a, b). In addition to difficulties in the experimental data base and in modeling ternary feldspar activities (Johannes 1979; Brown and Parsons 1981), it has been noted for many years that tie lines connecting coexisting feldspars from trachytes, phonolites, and other alkaline volcanic rocks typically have a much different orientation than tie lines for calc-alkaline rhyolites; for a given alkali feldspar composition, plagioclase tends to be considerably more calcic in alkaline rocks (Carmichael 1965; Rahman and McKenzie 1969; Carmichael et al. 1974, pp. 225–227; Stormer 1975; Ghiorso 1984). Ghiorso (1984) suggests that this divergence of tie lines is caused by resorption of plagioclase in alkaline magmas prior to eruption, and that the coexisting feldspars are not equilibrium pairs. We believe that the textural and compositional data cited above negate this explanation in the case of BLT pumices.

Current formulations of the two-feldspar geothermometer cannot be expected to give meaningful results for coexisting feldspars whose tie-lines deviate significantly from those of Seck (1971a and b). Coexisting plagioclase ($An_{89}$) and sanidine ($Or_{86}$) in most BLT pumices (Table 3; Fig. 3) are much richer in Ca and K, respectively, than coexisting feldspars from phonolites and trachytes reported in the literature. BLT plagioclases far exceed the $An_{55}$ limit cited by Stormer (1975) for "...virtually all plagioclase feldspars which coexist in nature with alkali feldspar...". Similar high-Ca plagioclase in association with high-K sanidine have been reported from cumulate monzonite and syenite nodules at Roccamonfina (Giannetti 1982), and phonolites from Roccamonfina (Giannetti 1974) and from Somma-Vesuvius (Barberi et al. 1981), and appear to be common at Italian volcanoes. Feldspars from BLT sample 226 and other basic BLT pumices have $X_{Na,san} > X_{Na,plag}$, and fall on the 'forbidden' side of the $X_{Na,san} = X_{Na,plag}$ line of graphical two-feldspar geothermometers (Brown and Parsons 1981). These BLT tie-lines cross at a slight angle tie-lines of Seck (1971a, b) and Ghiorso (1984). These formulations, therefore, cannot be applied to the majority of BLT feldspar analyses. We re-emphasize our belief that these are equilibrium feldspar pairs despite the inability of present ternary feldspar solution models to constrain their formation.

The evolved BLT sample 328-2 contains considerably more-sodic feldspars (Table 3) plus minor quantities of Ca-plagioclase and K-sanidine which are viewed as xenocrysts. The tie-line for the coexisting sodic feldspars is subparallel to those from Seck (1971a and b) and Ghiorso (1984) and the graphical geothermometer of Brown and Parsons (1981, Fig. 2) indicates an approximate temperature of 750° C.

*Xenocrystic diopside and olivine*

Besides the BLT, coexisting green salite and colorless diopside crystals are present in WTT pumices (Giannetti and Luhr 1983a), KS lavas (Ghiara and Lirer 1977; Ghiara et al. 1979), HKS lavas (unpublished data), and cumulate pyroxenite, monzonite, and syenite nodules (Giannetti 1982) from Roccamonfina, as well as in a wide spectrum of alkaline volcanic rocks from Italy and elsewhere (Thompson 1977; Brooks and Printzlau 1978; Barberi et al. 1981; Barton and van Bergen 1981; Civetta et al. 1981; Vollmer et al. 1981; Barton et al. 1982; Duda and Schmincke 1985). Most previous studies have attributed the coexistence of these two clinopyroxene populations to magma mixing prior to eruption, although alternative hypotheses have been postulated: polybaric crystallization (Ghiara and Lirer 1977; Ghiara et al. 1979; Duda and Schmincke 1985), disaggregation of wall rocks (Barton and van Bergen 1981), and reaction with carbonate country rocks (Barberi et al. 1981).

Most diopside crystals in BLT pumices are compositionally homogeneous, without mantles or rims of salite, the equilibrium clinopyroxene composition. In a few instances these diopside crystals were observed in clusters with forsteritic olivine ($Fo_{83-90}$: Table 6 and Fig. 7). Both of these phases are far too Mg-rich to have precipitated from BLT melts and are considered to be xenocrysts. Many of the xenocrysts probably formed through mixing of unerupted, primitive HKS magmas into the BLT magma chamber. The dark microcrystalline groundmass material surrounding some BLT xenocrysts (Fig. 6) probably represents a basic melt that was in equilibrium with these crystals and was partially quenched upon mixing into the cooler BLT magma. Bacon (1986) describes similar quenched clots of relatively basic magma in a variety of silicic and intermediate volcanic rocks. Some BLT diopsides show dissolution features indicating resorption in the mixed magmas, but the general lack of dissolution and of salite mantles is taken as evidence that these xenocrysts entered the BLT magma just prior to or during eruption. Many other workers have found evidence for mixing of magmas shortly before eruption (Anderson 1976; Johnston 1978; Sakuyama 1979 and 1981; Giannetti and Luhr 1983a; Worner and Wright 1984) and such mixing may in fact trigger explosive volcanic eruptions (Johnston and Schmincke 1977; Sparks et al. 1977), although it is not unequivocally possible to distinguish cause from effect in most cases.

One olivine xenocryst contains serpentine-filled fractures that undoubtedly formed by alteration of a solidified (cumulate?) rock at depth beneath Roccamonfina. Phlogopite pyroxenite nodules at Roccamonfina (Giannetti 1982) have olivine and diopside compositions that closely match those of BLT xenocrysts. Thus we find evidence for both cumulate disaggregation and magma mixing in the origin of diopside and olivine xenocrysts in BLT pumices. Worner and Wright (1984) envision mixing between late-stage Laacher See phonolites and a primary basanite containing mantle-derived wehrlite xenoliths to explain the presence of diopside and forsteritic olivine crystals in hybrid rocks. Such a model is also possible for the BLT xenocrysts, although pyroxenites have never been found within lavas at Roccamonfina. We also find evidence for repetitions of these xenocryst-generation events in the compositional zoning patterns of individual clinopyroxene crystals. Diopside cores mantled by salite (Fig. 5) represent earlier-generation xenocrysts that were overgrown by the stable salite composition prior to eruption. The most complex crystals show up to three repetitions of diopside/salite zones on a core-to-rim traverse. By the logic of our interpretation, these crystals must have alternately resided in basic and evolved melts. A specific scenario for such behavior, however, is admittedly difficult to envision.

*Origin of compositional zoning in the BLT*

It is now well established that most major pyroclastic eruptions display systematic changes toward more basic magma compositions and mineralogies with time (Smith and Bailey 1965; Smith 1979; Hildreth 1979, 1981, and 1983). These

**Table 10.** Crystal-fractionation model for deriving sample 328-2 from parent 47M

$\sum r^2 = 0.03$

| Mineral | wt% crystallized |
|---|---|
| Sanidine | 29.31 |
| Salite | 17.73 |
| Plagioclase | 7.70 |
| Biotite | 3.36 |
| Titanomagnetite | 2.97 |
| Apatite | 0.64 |
| | 61.06 |

| | Trace element concentrations in 328-2 | |
|---|---|---|
| | Observed | Predicted |
| Sc[a] | 1.70 (0.02) | <0.1 |
| Cr | 5.9 (0.7) | 3.3 – 16.5 |
| Co[a] | 2.2 (0.1) | <0.1 |
| Rb[a] | 405 (20) | 784 –967 |
| Sr | 316 (16) | 56 –505 |
| Ba | 177 (18) | 44 –337 |
| La | 164 (2) | 165 –189 |
| Ce[a] | 275 (2) | 308 –341 |
| Sm | 8.16 (0.08) | 3.6 – 10.2 |
| Eu | 1.25 (0.01) | 0.7 – 2.1 |
| Tb[a] | 0.59 (0.02) | 0.19– 0.37 |
| Yb | 3.93 (0.04) | 3.4 – 4.0 |
| Lu | 0.55 (0.03) | 0.55– 0.70 |
| Hf[a] | 10.17 (0.09) | 11.4 – 12.4 |
| Ta[a] | 1.41 (0.01) | 3.0 – 3.1 |
| Th[a] | 104 (1) | 97 – 99 |
| U[a] | 24.3 (0.2) | 19.6 – 20.2 |

[a] Observed value is not bracketed by predicted range

Mineral analyses: feldspars from sample 226 (Table 3), salite (*d*) from Table 6, biotite (47M) and apatite from Table 4, and titanomagnetite (47M) from Table 5. Partition coefficients from Upper Laacher See Tephra (Worner et al. 1983) and apatite from Luhr et al. (1984)

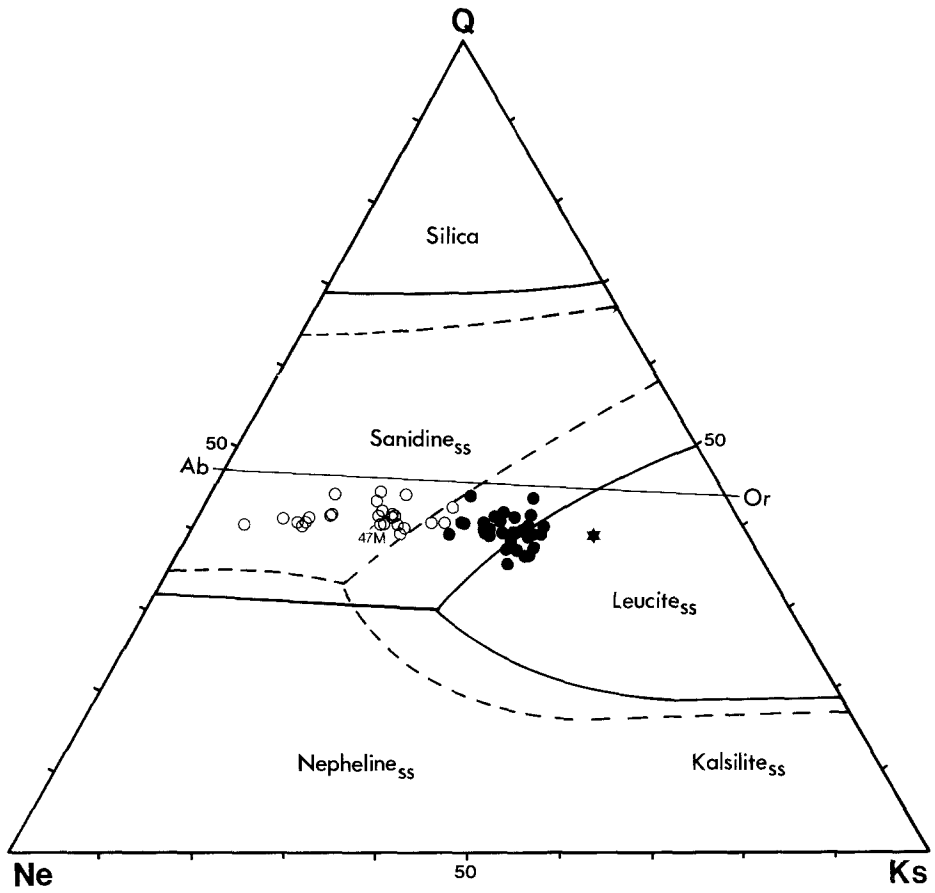


**Fig. 10.** Ternary system Quartz-Nepheline-Kalsilite (wt%) with cotectics for $P_{H_2O} = 1000$ bars (*solid lines*) taken from Hamilton and MacKenzie (1965) and for anhydrous conditions (*dashed lines*) taken from Fudali (1963). *Solid circles* represent BLT pumices with $< 5.6$ wt% CaO and *open circles* represent BLT pumices with $> 5.6$ wt% CaO. *Star* indicates assumed primary composition of sample 47M corrected for $Na_2O$ and $K_2O$

systematic zonations are generally interpreted to represent progressive emptying of a compositionally stratified magma chamber. Although the specific petrogenetic mechanisms that produce these gradients continue to be debated, crystal fractionation in the form of side-wall crystallization or actual crystal settling has been strongly supported in many recent investigations (Michael 1983a, b; Cameron 1984; Wolff and Storey 1984). The pioneering studies of such compositionally zoned pyroclastic eruptions focused on deposits in the western USA and consequently the data base was heavily biased toward calc-alkaline systems. More recent studies have expanded the debate to include alkaline magma systems (Mahood 1981; Giannetti and Luhr 1983a, b; Wolff and Storey 1984; Worner and Schmincke 1984a, b).

Interpretation of BLT petrogenesis is complicated by the almost complete analcimization of leucite that has affected all pumices, but particularly the more basic samples ($> 5.6$ wt% CaO), which contain a large number of secondary analcime crystals in their matrices. The lowered whole-rock $K_2O$ and increased $Na_2O$ contents of these pumices are apparent both on Fig. 8 and on Fig. 10, a plot of the ternary system Quartz-Nepheline-Kalsilite with cotectics for $P_{H_2O} = 1000$ bars (solid lines) and anhydrous conditions (dashed lines). BLT pumices with $< 5.6$ wt% CaO (solid dots) straddle the sanidine-leucite cotectic for $P_{H_2O} = 1000$ bars, appropriate to their primary mineralogy, whereas pumices with $> 5.6$ wt% CaO (open circles) scatter across the sanidine field with much higher Na/K ratios. The coincidence of evolved BLT pumice compositions with the 1000-bar cotectic is taken as support for crystallization of the BLT under similar water pressures prior to eruption. The effects of water pressure and total pressure on the cotectic position, however, can not be independently evaluated from the existing experimental data base.

In modeling compositional variations among BLT pumices we have corrected alkali abundances in the basic samples to resemble HKS lavas of similar CaO content. Values for the most-CaO-rich BLT pumice 47M (2.2% $Na_2O$ and 8.0% $K_2O$) are shown as stars on Figs. 8 and 10. These values are relatively arbitrary within the rather wide variations present among HKS lavas of similar CaO content (Fig. 8). This phonolitic leucite-tephrite was tested using least-squares techniques (Stormer and Nicholls 1978) as a parent composition for deriving the more-evolved BLT pumices. A model for deriving the most-evolved sample 328-2 is given in Table 10. Mineral compositions typical of basic BLT pumices were used. The model calls for 61 wt% crystallization of a sanidine-salite-dominated assemblage. The relative proportions of predicted minerals are very similar to the modes of cumulate monzonite and syenite nodules which are quite abundant in the BLT and other pyroclastic formations at Roccamonfina (Giannetti 1982). The compositions of BLT minerals also closely match those from monzonite and syenite nodules. A more-evolved syenite assemblage richer in sanidine was predicted in a similar model for deriving observed compositional variations among WTT pumices (Giannetti and Luhr 1983a). The fractionating assemblage modelled for the BLT is richer in feldspars and poorer in salite and biotite than the actual

modes of basic BLT pumices. This discrepancy may reflect the relative insensitivity of feldspar proportions in least squares models for evolved magmas, or an actual increase in the felsic/mafic ratio in the portion of the BLT magma system (sidewall?) where fractionation took place.

The predicted mineral proportions were used to test variations for 17 trace elements among BLT pumices assuming Rayleigh fractionation (Arth 1976). Trace element partition coefficients were taken from the more-basic phonolites of the highly sodic Upper Laacher See Tephra (Worner et al. 1983). The single apatite analysis in that set was augmented by apatite partition coefficients from the El Chichon trachyandesite (Luhr et al. 1984). The observed ranges in partition coefficients result in concentration ranges for each modeled trace element in sample 328-2 (Table 10). The model is successful, with the predicted range bracketing the observed value, for eight elements including Sr, Ba, and most REEs. The model is unsuccessful for nine elements. The compatible elements Sc and Co are present in higher concentrations than predicted. This may reflect the presence of a physically mixed, basic component in all BLT pumices as indicated by ubiquitous diopside and olivine xenocrysts. The predicted concentrations of Rb are much too high, but consistent with the known enrichment of Rb during analcimization of leucite (Fornaseri and Penta 1960). Among REEs, Ce is overpredicted and Tb is underpredicted, yet the overall shape of the REE pattern is very similar to that of 328-2 (Fig. 9). A slight decrease in the high Laacher See clinopyroxene partition coefficients for Tb (6.8–8.6) can bring this element into harmony. Th and U are underpredicted by >5% and >20% respectively, whereas Hf (>11%) and especially Ta (>53%) are overpredicted. These latter deviations may reflect very minor crystallization of sphene, which has very high partition coefficients for Hf (4.9–13.4) and particularly Ta (86–142) (Worner et al. 1983; Luhr et al. 1984). Sphene was never observed in heavy mineral concentrations from BLT pumices, but a few crystals were seen in thin section, and sphene is usually present in at least trace quantities in phonolites (Giannetti 1970, 1974) and in monzonite and syenite nodules at Roccamonfina (Giannetti 1982). Minor sphene fractionation would lower REE values in the model, but should not change the above interpretations significantly. Major and trace element variations among BLT pumices closely parallel those for phonolitic pumices from the 79 A.D. eruption of nearby Somma-Vesuvius (Barberi et al. 1981; Wolff and Storey 1984). The only significant differences between the two suites are noted in trends for Y, Yb, and Lu, which behave as compatible elements in Somma-Vesuvius samples, but as incompatible elements in BLT pumices. These differences are easily explained by the presence of garnet in Somma-Vesuvius pumices (Barberi et al. 1981) and its absence in BLT pumices.

As mentioned in the last section, CaO variation plots show a slight gap at about 3.8% CaO, where Zr, Ba, and Sr trends also show a change in slope (Fig. 8). These deflections may indicate an increase in the feldspar/salite or sanidine/plagioclase ratios in the fractionating assemblage, either of which would lead to steepening of trends for Zr, Ba, and Sr versus CaO. Such changes in the proportions of fractionating minerals may in turn reflect a two-stage ascent of the BLT magma. CaO contents down to about 3.8% may have been generated at relatively higher pressures. Such a magma may then have ascended to a higher position in the plumbing system of Roccamonfina, where the more evolved magmas (<3.8% CaO) formed through fractionation of an assemblage richer in either sanidine or total feldspar.

With consideration of uncertainties involved in correcting alkali contents of basic BLT pumices and in the use of trace element partition coefficients from the highly sodic Laacher See Tephra, we believe that the crystal fractionation model in Table 10 is successful. The model is most convincing due to the similarity of predicted mineral abundances and compositions to those actually observed in cumulate monzonites and syenites carried to the surface by the BLT eruption. Over 30 analyses of Sr isotopic composition have been published for HKS lavas of Roccamonfina, along with lesser numbers of Nd and Pb isotopic data (Cox et al. 1976; Vollmer 1976; Carter et al. 1978; Hawkesworth and Vollmer 1979; Vollmer and Hawkesworth 1980; Vollmer et al. 1981). Although the various isotopic systems show well-correlated ratios, both whole-rock Sr contents and $^{87}Sr/^{86}Sr$ in HKS lavas display wide variations when plotted versus CaO or other indices of fractionation. The wide variations in $^{87}Sr/^{86}Sr$ (0.7083–0.7099) and other isotopic ratios indicate that the spectrum of HKS magmas can not be generated by simple crystal fractionation. Most isotopic analyses of HKS lavas were performed on samples studied by Appleton (1972), and specific genetic relationships among them can not be demonstrated in the field. Future isotopic study of phases from BLT pumices, in which whole-rock Sr, Nd and Pb concentrations smoothly vary with CaO, will confirm or deny our simple crystal fractionation model.

*Acknowledgements.* We are indebted to Al Deino and Bob Drake of the Berkeley Geochronology Center for K-Ar dating of the BLT and to Helen Michel, Rodey Batiza, and Pat Castillo for facilitating INA analyses. The manuscript was improved significantly through critiques by Gerhard Wörner and an anonymous reviewer. B.G. expresses his gratitude to Comitato 05 of CNR for supporting a 2 month stay in the USA. However, the majority of the field work was conducted with his personal funds.

## References

Anderson AT (1976) Magma mixing: petrological process and volcanological tool. J Volcanol Geotherm Res 1:3–33

Appleton JD (1972) Petrogenesis of potassium-rich lavas from Roccamonfina Volcano, Roman Region, Italy. J Petrol 133:425–456

Arth JG (1976) Behavior of trace elements during magmatic processes – A summary of theoretical models and their applications. US Geol Surv J Res 4-1:41–47

Bacon CR (1986) Magmatic inclusions in silicic and intermediate volcanic rocks. J Geophys Res 91, B6:6091–6112

Barberi F, Innocenti F, Lirer L, Munno R, Pescatore T, Santacroce R (1978) The Campanian Ignimbrite: a major prehistoric eruption in the Neopolitan area (Italy). Bull Volcanol 41:1–22

Barberi F, Bizouard H, Clocchiatti R, Metrich N, Santacroce R, Sbrana A (1981) The Somma-Vesuvius magma chamber: a petrological and volcanological approach. Bull Volcanol 44-3:295–315

Barberi F, Innocenti F, Lirer L, Munno R, Pescatore T, Santacroce R (1983) Compositional variations in the Campanian Ignimbrite, Italy: Hydrothermal modification of pre-eruptive fractionation. Bull Volcanol 46-4:433–434

Barton M, van Bergen, MJ (1981) Green clinopyroxenes and associated phases in a potassic-rich lava from the Leucite Hills, Wyoming. Contrib Mineral Petrol 77:101–114

Barton M, Varekamp JC, Van Bergen MJ (1982) Complex zoning in clinopyroxenes in the lavas of Vulsini, Latium, Italy: Evidence for magma mixing. J Volcanol Geotherm Res 14:361–388

Bergomi C, Catenacci V, Cestari G, Manfredini M, Manganelli V (1969) Note illustrative della carta geologica d'Italia. Foglio 171:Gaeta e Vulcano di Roccamonfina. Serv Geol d'Italia

Blake S (1981) Eruptions from zoned magma chambers. J Geol Soc Land 138:281–287

Brooks CK, Printzlau I (1978) Magma mixing in mafic alkaline volcanic rocks: The evidence from relict phenocryst phases and other inclusions. J Volcanol Geotherm Res 4:315–331

Brown WL, Parsons I (1981) Towards a more practical two-feldspar geothermometer. Contrib Mineral Petrol 76:369–377

Cameron KL (1984) Bishop Tuff revisited: New rare earth element data consistent with crystal fractionation. Science 224:1338–1340

Carmichael ISE (1965) Trachytes and their feldspar phenocrysts. Mineral Mag 34–268:107–125

Carmichael ISE (1967) The iron-titanium oxides of salic volcanic rocks and their associated ferromagnesian silicates. Contrib Mineral Petrol 14:36–64

Carmichael ISE, Turner FJ, Verhoogen J (1974) Igneous Petrology. McGraw-Hill, New York, p 739

Carter SR, Evensen NM, Hamilton PJ, O'Nions RK (1978) Continental volcanics derived from enriched and depleted source regions: Nd- and Sr-isotope evidence. Earth Planet Sci Lett 37:401–408

Chiesa S, Cornette Y, Gillot PY, Vezzoli L (1985) New interpretation of Roccamonfina volcanic history. IAVCEI, Sicily, abstract

Civetta L, Innocenti F, Manetti P, Peccerillo A, Poli G (1981) Geochemical characteristics of potassic volcanics from Mts. Ernici (Southern Latium, Italy). Contrib Mineral Petrol 78: 37–47

Cornell WC, Sigurdsson H, Sparks RSJ (1979) The Campanian Ignimbrite of SW Italy: Eruptive phases and variations in glass chemistry. Trans Am Geophys Un EOS 60 18:409

Cortini M, Roberti N, Scandone R (1975) Geocronologia e paleomagnetismo del vulcano di Roccamonfina. Ann Geofys 28:129–138

Cox KG, Hawkesworth CJ, O'Nions RK, Appleton JD (1976) Isotopic evidence for the derivation of some Roman Region volcanics from anomalously enriched mantle. Contrib Mineral Petrol 56:173–180

Di Girolamo P (1968) Rilevamento petrografico nel settore SW (Sessa Aurunca) del Vulcano di Roccamonfina. Rend Acc Sci Fis Mat Napoli 4 35:675–722

Di Girolamo P (1970) Differenziazione gravitativa e curve isochimiche nella ignimbrite Campana. Rend Soc Ital Mineral Petrol 26-2:547–588

Duda A, Schmincke H-U (1985) Polybaric differentiation of alkali basaltic magmas: Evidence from green-core clinopyroxenes (Eifel, FRG). Contrib Mineral Petrol 91:340–353

Evernden JF, Curtis GH (1965) The potassium-argon dating of late Cenozoic rocks in East Africa and Italy. Curr Anthrop 6:343–364

Fitton JG, Upton BGJ (1985) Alkaline igneous rocks: a review symposium. J Geol Soc Lond 142:697–708

Fornaseri M, Penta A (1960) Elementi alcalini minori negli analcimi e loro comportamento nel processo di analcimizzazione della leucite. Period Mineral (Roma) 29:85–102

Fudali RF (1963) Experimental studies bearing on the origin of pseudoleucite and associated problems of alkalic rock systems. Geol Soc Am Bull 74:1101–1126

Ghiara MR, Lirer L (1977) Mineralogy and geochemistry of the "Low-potassium" series of the Roccamonfina volcanic suite (Campania, South Italy). Bull Volcanol 41:39–56

Ghiara MR, Lirer L, Stanzione L (1973) Contributo alla conoscenza vulcanologica e petrografica del vulcano di Roccamonfina. Period Mineral 42:267–293

Ghiara MR, Lirer L, Munno R (1979) Mineralogy and geochemistry of the "Low-potassium" series of the Campania volcanics (South Italy). Chem Geol 26:29–49

Ghiorso MS (1984) Activity/composition relations in the ternary feldspars. Contrib Mineral Petrol 87:282–296

Giannetti B (1964) Contributo alla conoscenza del vulcano di Roccamonfina. Nota 1: Le ultime manifestazioni eruttive della caldera. Boll Soc Geol Ital 83-3:87–133

Giannetti B (1970) Contributo alla conoscenza delle lave leucitiche e delle piroclastiti della cinta calderica di Roccamonfina e petrochimica del complesso vulcanico. Mem Soc Geol Ital 9:497–556

Giannetti B (1974) Nuove ricerche petrografiche e petrogenetiche sulle lave fonolitiche della caldera vulcanica di Roccamonfina. Atti Soc Toscana Sci Nat Pisa Mem 81:253–306

Giannetti B (1979a) The geology of Roccamonfina caldera (Campanian Province, Italy). Giornale Geologia (Ser 2) 43:187–206

Giannetti B (1979b) Studio geologico-petrografico della caldera del vulcano di Roccamonfina (Italia centro-meridionale). Boll Serv Geol Ital 100:311–374

Giannetti B (1982) Cumulate inclusions from K-rich magmas, Roccamonfina volcano, Italy. Earth Planet Sci Lett 57:313–335

Giannetti B, Luhr JF (1983a) The White Trachytic Tuff of Roccamonfina Volcano (Roman Region, Italy). Contrib Mineral Petrol 84:235–252

Giannetti B, Luhr JF (1983b) Compositional variations in the Grey Campanian Ignimbrite, Italy: Hydrothermal modification or pre-eruptive fractionation? Bull Volcanol 46-4:429–431

Giannetti B, Nicoletti M, Petrucciani C (1979) Datazioni K-Ar di lave leucitiche dello strato-vulcano die Roccamonfina. Rend Soc Ital Mineral Petrol 35 1:349–354

Gupta AK, Fyfe WS (1975) Leucite survival: The alteration to analcime. Can Mineral 13:361–363

Hamilton DL, MacKenzie WS (1965) Phase equilibrium studies in the system $NaAlSiO_4$-$KAlSiO_4$-$SiO_2$-$H_2O$. Mineral Mag 34:214–231

Haselton HT Jr, Hovis GL, Hemingway BS, Robie RA (1983) Calorimetric investigation of the excess entropy of mixing in analbite-sanidine solid solutions: lack of evidence for Na, K short range order and implications for two-feldspar thermometry. Am Mineral 68:398–413

Hawkesworth CJ, Vollmer R (1979) Crustal contamination versus enriched mantle: $^{143}Nd/^{144}Nd$ and $^{87}Sr/^{86}Sr$ evidence from the Italian volcanics. Contrib Mineral Petrol 69:151–165

Hildreth W (1979) The Bishop Tuff: Evidence for the origin of compositional zonation in silicic magma chambers. In: Chapin CE, Elston WE (eds) Ash-flow tuffs. Geol Soc Am Spec Pap 180:43–75

Hildreth W (1981) Gradients in silicic magma chambers: implications for lithosphere magmatism. J Geophys Res 86:10153–10192

Hildreth W (1983) Comment – Chemical differentiation of the Bishop Tuff and other high-silica magmas through crystallization processes. Geology 11:622–623

Jacobs JW, Korotev RL, Blanchard DP, Haskin LA (1977) A well-tested procedure for instrumental neutron activation analysis of silicate rocks and minerals. J Radioanal Chem 40:93–114

Johannes W (1979) Ternary feldspars: Kinetics and possible equilibria at 800° C. Contrib Mineral Petrol 68:221–230

Johnston DA, Schmincke H-U (1977) Triggering of explosive volcanic eruptions by mixing of basaltic and silicic magmas. Geol Soc Am Abstr Prog:1041

Johnston DA (1978) Volatiles, magma mixing, and the mechanism of eruption of Augustine Volcano, Alaska. Univ Wash, Unpubl PhD dissert, p 177

Lindstrom DJ, Korotev RL (1982) TEABAGS: Computer programs for instrumental neutron activation analysis. J Radioanal Chem 70:439–458

Luhr JF, Carmichael ISE, Varekamp JC (1984) The 1982 eruptions of El Chichon Volcano, Chiapas, Mexico: Mineralogy and petrology of the anhydrite-bearing pumices. J Volcanol Geotherm Res 23:69–108

Mahood G (1981) Chemical evolution of a Pleistocene rhyolitic center: Sierra La Primavera, Jalisco, Mexico. Contrib Mineral Petrol 77:129–149

Masuda A, Nakamura N, Tanaka T (1973) Fine structures of mutually normalized rare-earth patterns of chondrites. Geochim Cosmoch Acta 37:239–248

Michael PJ (1983a) Chemical differentiation of the Bishop Tuff and other high-silica magmas through crystallization processes. Geology 11:31–34

Michael PJ (1983b) Reply – Chemical differentiation of the Bishop Tuff and other high-silica magmas through crystallization processes. Geology 11:623–624

Nielsen CH, Sigurdsson H (1981) Quantitative methods for electron microprobe analysis of sodium in natural and synthetic glasses. Am Mineral 66:547–552

Passaglia E, Vezzalini G (1985) Crystal chemistry of diagenetic zeolites in volcanoclastic deposits of Italy. Contrib Mineral Petrol 90:190–198

Peccerillo A, Poli G, Tolomeo L (1984) Genesis, evolution and tectonic significance of K-rich volcanics from the Alban Hills (Roman comagmatic region) as inferred from trace element geochemistry. Contrib Mineral Petrol 86:230–240

Perlman I, Asaro F (1969) Pottery analysis by neutron activation. Archaeometry 11:21–52

Rahman S, MacKenzie WS (1969) The crystallization of ternary feldspars: A study from natural rocks. Am J Sci 267-A:391–406

Rittmann A (1973) Stable mineral assemblages of igneous rocks. Springer Berlin

Rogers NW, Hawkesworth CJ, Parker RJ, Marsh JS (1985) The geochemistry of potassic lavas from Vulsini, central Italy and implications for mantle enrichment processes beneath the Roman region. Contrib Mineral Petrol 90:244–257

Rose HJ, Adler I, Flanagan FJ (1963) X-ray fluorescence analysis of the light elements in rocks and minerals. Appl Spectrosc 17:81–85

Sakuyama M (1979) Evidence of magma mixing: petrological study of Shirouma-Oike calc-alkaline andesite volcano, Japan. J Volcanol Geotherm Res 5:197–208

Sakuyama M (1981) Petrological study of Myoko and Kurohime Volcanoes, Japan: Crystallization sequence and evidence for magma mixing. J Petrol 22-4:553–583

Seck HA (1971a) Koexistierende Alkalifeldspate und Plagioklase im System $NaAlSi_3O_8$-$KAlSi_3O_8$-$CaAl_2Si_2O_8$-$H_2O$ bei Temperaturen von 650° C bis 900° C. Neues Jahrb Mineral Abh 115:315–345

Seck HA (1971b) Der Einfluß des Drucks auf die Zusammensetzung koexistierender Alkalifeldspate und Plagioklase im System $NaAlSi_3O_8$-$KAlSi_3O_8$-$CaAl_2Si_2O_8$-$H_2O$. Contrib Mineral Petrol 31:67–86

Smith RL (1979) Ash-flow magmatism. In: Chapin CE, Elston WE (eds) Ash-flow tuffs. Geol Soc Am Spec Pap 180:5–27

Smith RL, Bailey RA (1965) The Bandelier Tuff: a study of ash flow eruption cycles from zoned magma chambers. Bull Volcanol 29:83–103

Sparks SRJ (1975) Stratigraphy and geology of the ignimbrites of Vulsini Volcano, Central Italy. Geol Rundsch 64:497–523

Sparks RSJ, Self S, Walker GPL (1973) Products of ignimbrite eruptions. Geology 1:115–118

Sparks RSJ, Sigurdsson H, Wilson L (1977) Magma mixing: a mechanism for triggering acid explosive eruptions. Nature 267:315–318

Spera FJ, Yuen DA, Greer JC, Sewell G (1986) Dynamics of magma withdrawal from stratified magma chambers. Geology 14:723–726

Stormer JC Jr (1975) A practical two-feldspar geothermometer. Am Mineral 60:667–674

Stormer JC Jr, Nicholls J (1978) XLFRAC: A program for interactive testing of magmatic differentiation models. Computer Geosci 4:143–159

Streckeisen AL (1967) Classification and nomenclature of igneous rocks. Neues Jahrb Mineral Abh 107, 2:144–214

Tedesco C (1964) Main lines of the history of Roccamonfina Volcano. Bull Volcanol 28:119–141

Thompson RN (1977) Primary basalts and magma genesis – III. Alban Hills, Roman Comagmatic Province, Central Italy. Contrib Mineral Petrol 60:91–108

Varekamp JC (1980) The geology of the Vulsini area, Lazio, Italy. Bull Volcanol 43-3:487–505

Vollmer R (1976) Rb-Sr and U-Th-Pb systematics of alkaline rocks: the alkaline rocks from Italy. Geochim Cosmoch Acta 40:283–295

Vollmer R, Hawkesworth CJ (1980) Lead isotopic composition of the potassic rocks from Roccamonfina (South Italy). Earth Planet Sci Lett 47:91–101

Vollmer R, Johnston K, Ghiara MR, Lirer L, Munno R (1981) Sr isotope geochemistry of megacrysts from continental rift and converging plate margin alkaline volcanism in south Italy. J Volcanol Geotherm Res 11:317–327

Whittaker EJW, Muntus R (1970) Ionic radii for uses in geochemistry. Geochim Cosmoch Acta 34:945–956

Wilkinson JFG (1977) Analcime phenocrysts in a vitrophyric analcimite – primary or secondary? Contrib Mineral Petrol 64:1–10

Wolff JA, Storey M (1984) Zoning in highly alkaline magma bodies. Geol Mag 121-6:563–575

Wörner G, Wright TL (1984) Evidence for magma mixing within the Laacher See magma chamber (East Eifel, FRG). J Volcanol Geotherm Res 22:301–327

Worner G, Schmincke H-U (1984a) Mineralogical and chemical zonation of the Laacher See Tephra sequence (East Eifel, FRG). J Petrol 25-4:805–835

Worner G, Schmincke H-U (1984b) Petrogenesis of the zoned Laacher See tephra. J Petrol 25-4:836–851

Worner G, Beusen J-M, Duchateau N, Gijbels R, Schmincke H-U (1983) Trace element abundances and mineral/melt distribution coefficients in phonolites from the Laacher See Volcano (FRG). Contrib Mineral Petrol 84:152–173

Received March 17, 1986 / Accepted December 23, 1986